FINAL REPORT ~ FHWA-OK-22-04

SHRINKAGE INDUCED DEFORMATIONS IN STEEL BRIDGES MADE COMPOSITE WITH CONCRETE DECK SLABS

Bruce W. Russell, Ph.D., P.E., S.E., F.ACI
Alla Eddine Acheli, BSCE, MSCE
Hema Jayaseelan, MSCE, Ph.D., P.E.
Anna Corelle Webb, MSCE, P.E.
Ibrahim S. Abdelmeguid, P.E.
Kendall Belcher, MSCE
Chris Filip, BSCE

Civil Engineering and Environmental Science
Oklahoma State University
Stillwater, Oklahoma

March 2022

OKLAHOMA Transportation

The Oklahoma Department of Transportation (ODOT) ensures that no person or groups of persons shall, on the grounds of race, color, sex, religion, national origin, age, disability, retaliation or genetic information, be excluded from participation in, be denied the benefits of, or be otherwise subjected to discrimination under any and all programs, services, or activities administered by ODOT, its recipients, sub-recipients, and contractors. To request an accommodation please contact the ADA Coordinator at 405-521-4140 or the Oklahoma Relay Service at 1-800-722-0353. If you have any ADA or Title VI questions email ODOT-ada-titlevi@odot.org.

SHRINKAGE INDUCED DEFORMATIONS IN STEEL BRIDGES MADE COMPOSITE WITH CONCRETE DECK SLABS

FINAL REPORT – FHWA – OK-22-04
ODOT SP&R ITEM NUMBER 2260

Submitted to:

Office of Research and Implementation
Oklahoma Department of Transportation

Submitted by:

Bruce W. Russell, Ph.D., P.E., S.E., F.ACI
Alla Eddine Acheli, BSCE, MSCE
Hema Jayaseelan, MSCE, Ph.D., P.E.
Anna Corelle Webb, MSCE, P.E.
Ibrahim S. Abdelmeguid, P.E.
Kendall Belcher, MSCE
Chris Filip, BSCE

Civil Engineering and Environmental Science
Oklahoma State University

OKLAHOMA
Transportation

March 2022

TECHNICAL REPORT DOCUMENTATION PAGE

1. REPORT NO. FHWA-OK-22-04	2. GOVERNMENT ACCESSION NO.	3. RECIPIENT'S CATALOG NO.	
4. TITLE AND SUBTITLE Shrinkage Induced Deformations in Steel Bridges Made Composite with Concrete Deck Slabs		5. REPORT DATE Mar 2016	
		6. PERFORMING ORGANIZATION CODE	
7. AUTHOR(S) Bruce W. Russell, A.E. Acheli, Hema Jayaseelan, A. Corelle Webb, I. S. Abdelmeguid, K. Belcher, C. Filip		8. PERFORMING ORGANIZATION REPORT College of Engineering, Architecture and Technology	
9. PERFORMING ORGANIZATION NAME AND ADDRESS School of Civil and Environmental Engineering Oklahoma State University Engineering North 245 Stillwater, OK 74048		10. WORK UNIT NO.	
		11. CONTRACT OR GRANT NO. ODOT SPR Item Number 2260	
12. SPONSORING AGENCY NAME AND ADDRESS Oklahoma Department of Transportation Office of Research and Implementation 200 N.E. 21st Street, Room G18 Oklahoma City, OK 73105		13. TYPE OF REPORT AND PERIOD COVERED Final Report Example: Oct 2014 - Dec 2022	
		14. SPONSORING AGENCY CODE	
15. SUPPLEMENTARY NOTES Click here to enter text.			
16. ABSTRACT Concrete bridge deck cast upon steel girders form a composite steel-concrete bridge. Volume changes in the concrete caused by shrinkage, temperature or other effects can alter the finished elevations of the bridge decks. Some of the state's newly constructed bridges have experienced downward deflecting decks, causing uneven riding surfaces. It has been suggested by some that the excessive deflections are caused by drying shrinkage of concrete. The research investigated the shrinkage characteristics of concrete, examined analytically the likely effects of concrete shrinkage on composite steel and concrete girder bridges, examined experimentally the system of concrete and steel bridge beams, and performed forensic field investigations of existing bridges. In various phases, material properties of concrete were studied, and a full-scale prototype bridge was constructed in the laboratory. That bridge was used to examine bridge deformations during deck casting and curing. The bridge was tested with heat loads and results are reported. Causes for excessive deflections are examined. It is concluded that the construction means and methods are largely responsible for unwanted bridge deformations and poor ride quality in some new bridges. Recommendations are made to the ODOT to help mitigate adverse effects.			
17. KEY WORDS Steel Bridges, Composite, Concrete Deck, Curing, Ride Quality,		18. DISTRIBUTION STATEMENT No restrictions. This publication is available from the Office of Research and Implementation, Oklahoma DOT.	
19. SECURITY CLASSIF. (OF THIS REPORT) Unclassified	20. SECURITY CLASSIF. (OF THIS PAGE) Unclassified	21. NO. OF PAGES 82	22. PRICE N/A

SI* (MODERN METRIC) CONVERSION FACTORS

APPROXIMATE CONVERSIONS TO SI UNITS

SYMBOL	WHEN YOU KNOW	MULTIPLY BY	TO FIND	SYMBOL
LENGTH				
in	inches	25.4	millimeters	mm
ft	feet	0.305	meters	m
yd	yards	0.914	meters	m
mi	miles	1.61	kilometers	km
AREA				
in^2	square inches	645.2	square millimeters	mm^2
ft^2	square feet	0.093	square meters	m^2
yd^2	square yard	0.836	square meters	m^2
ac	acres	0.405	hectares	ha
mi^2	square miles	2.59	square kilometers	km^2
VOLUME				
fl oz	fluid ounces	29.57	milliliters	mL
gal	gallons	3.785	liters	L
ft^3	cubic feet	0.028	cubic meters	m^3
yd^3	cubic yards	0.765	cubic meters	m^3
NOTE: volumes greater than 1000 L shall be shown in m^3				
MASS				
oz	ounces	28.35	grams	g
lb	pounds	0.454	kilograms	kg
T	short tons (2000 lb)	0.907	megagrams (or "metric ton")	Mg (or "t")
TEMPERATURE (exact degrees)				
°F	Fahrenheit	5 (F-32)/9 or (F-32)/1.8	Celsius	°C
ILLUMINATION				
fc	foot-candles	10.76	lux	lx
fl	foot-Lamberts	3.426	candela/m^2	cd/m^2
FORCE and PRESSURE or STRESS				
lbf	poundforce	4.45	newtons	N
lbf/in^2	poundforce per square inch	6.89	kilopascals	kPa

APPROXIMATE CONVERSIONS FROM SI UNITS

SYMBOL	WHEN YOU KNOW	MULTIPLY BY	TO FIND	SYMBOL
LENGTH				
mm	millimeters	0.039	inches	in
m	meters	3.28	feet	ft
m	meters	1.09	yards	yd
km	kilometers	0.621	miles	mi
AREA				
mm^2	square millimeters	0.0016	square inches	in^2
m^2	square meters	10.764	square feet	ft^2
m^2	square meters	1.195	square yards	yd^2
ha	hectares	2.47	acres	ac
km^2	square kilometers	0.386	square miles	mi^2
VOLUME				
mL	milliliters	0.034	fluid ounces	fl oz
L	liters	0.264	gallons	gal
m^3	cubic meters	35.314	cubic feet	ft^3
m^3	cubic meters	1.307	cubic yards	yd^3
MASS				
g	grams	0.035	ounces	oz
kg	kilograms	2.202	pounds	lb
Mg (or "t")	megagrams (or "metric ton")	1.103	short tons (2000 lb)	T
TEMPERATURE (exact degrees)				
°C	Celsius	1.8C+32	Fahrenheit	°F
ILLUMINATION				
lx	lux	0.0929	foot-candles	fc
cd/m^2	candela/m^2	0.2919	foot-Lamberts	fl
FORCE and PRESSURE or STRESS				
N	newtons	0.225	poundforce	lbf
kPa	kilopascals	0.145	poundforce per square inch	lbf/in^2

*SI is the symbol for the International System of Units. Appropriate rounding should be made to comply with Section 4 of ASTM E380. (Revised March 2003)

Table of Content:

List of Figures:

List of Tables:

1. EXECUTIVE SUMMARY

This the Final report concentrates on work performed since the beginning of the project and findings from FY21. More detailed information on Phase 1, Phase 2 and part of Phase 3 activities can be found in the annual reports from FY15, FY16, FY17, FY18, FY19 and FY20 Annual Reports.

Concrete bridge decks are typically cast upon steel or precast concrete girders. New concrete, upon taking initial set begins to change volume. Volume changes are caused by temperature changes, creep or drying shrinkage. Theoretically, compressive strains cause bridge members to deflect downward. Some of Oklahoma's recently re-constructed bridge decks experienced downward deflections at locations near mid spans that exceed engineering projections and cause adverse ride quality. Three recently constructed bridges in Woods Co. brought attention to this topic and heightened awareness of the need for this research. It has been suggested by some that the excessive deflections are caused by drying shrinkage of concrete.

In the Phase 1 of this research, laboratory testing was performed, an analytical model was developed, and forensic examinations were performed on three bridges. In laboratory testing, concrete materials were tested for compressive strength, elastic modulus, tensile strength and shrinkage. Prototype beams were cast and monitored for temperature, strains and deflections. In the Phase 2 of this research laboratory testing was performed on scale model prototype beams.

In 2016, laboratory testing was performed on the full-sized prototype beams. Additional load testing was performed on the bracing and formwork systems. From the data recorded it was evident that poor ride quality and poor elevation control of finished bridge decks is being caused principally by excessive deflections of the formwork and its bracing. This excessive deflection occurred most during placement of the fresh concrete as the bridge deck was being cast.

In the Phase 3 of this research, thermal loading was applied to the prototype bridge deck after 56 days of curing. Uniform heating of the deck caused a temperature gradient within the bridge deck resulting in differential strains and stresses at various location of the bridge deck. The results from the real time thermal loading on the prototype bridge decks showed that the temperature gradients produced internal thermal strains and stresses that directly resulted in bridge deformations. Computational analytical models were developed to predict and validate the stresses and strains developed in the composite cross-section of the prototype bridge. The models found good correlation with the measured overall bridge deflections.

The creep phenomenon in concrete is better understood in compression and not so much in tension. A new test method that can measure creep of concrete in tension was developed. Laboratory testing on various concrete mixes including ODOT AA concrete mix with and without fly ash, low w/cm and optimized graded concrete mixtures are being performed to determine the effects of both creep and shrinkage in concrete. This new test method will provide an improved understanding of the time-depended concrete properties that contributes to early age cracking.

Also as part of Phase 3, the steel girder bridge on SH 11 over the Chikaskia River was instrumented with thermocouples and vibrating wire strain gages during rehabilitation of the concrete deck. Instrumentation was placed on the bridge girders prior to demolition of the concrete deck and was maintained by a remote structural health monitoring system throughout

the complete deck rehabilitation. During this construction work, concrete material samples were made and tested, and temperatures of concrete and steel structural elements were measured, monitored, and recorded.

One of the most important recommendations that we derived from this research work is that the ODOT should no longer provide prescriptive information for bracing and formwork on design drawings for bridges. As documented in our reporting, the bracing systems are contributing to:

(1) Poor ride quality, where bridge deck elevations causes "humps" and "dips" in newly constructed bridge decks, and'
(2) Thin Bridge Decks. In some cases, bridge decks were measured less than 7 in. thickness where 8 in. had been prescribed.

Both of these adverse factors result directly from too much deflection in the bracing systems supporting cantilevered portions of formwork. These systems are PRESCRIBED, in many cases, by ODOT design drawings. These prescriptions on means and methods should no longer be placed on design drawings. Instead, bridge specifications should be modified to include performance specification of the final product where the means and methods of providing level riding surfaces are left to the contractor. This is done very well on paving projects. It is recommended that a similar approach be taken to elevation controls for bridge decks.

2. ACKNOWLEDGEMENTS

The APPENDIX to this Final Report includes three papers that have been published, or submitted to archival journals. Copies of these papers in their published format are included and made part of this Final Report.

The authors of various reports, papers and presentations are all current or former graduate students supported by the research funded by ODOT. These authors, and their faculty advisor, express their heartfelt and extraordinary gratitude to the ODOT for their support for University Research. As the Principal Investigator, and as the Academic Advisor to all of these students, it is my *(Bruce Russell's)* firm belief that one of the greatest contributions from ODOT-SPONSORED RESEARCH is the HUMAN CAPITAL that is developed through the ODOT funding. These students become Professional Engineers with special knowledge about materials, structures, and transportation systems. Furthermore, most of them continue their careers in transportation-related endeavors that BUILD CAPACITY and KNOWLEDGE in TRANSPORTATION. So, thank you from the bottoms of our hearts. I hope we always remain grateful.

In addition to the information contained in this Final Report, please also acknowledge the following presentations made to ODOT and University Transportation Research Days and to Local, State and National Conferences and meetings:

- Jayaseelan, H. and Russell, B.W. (2022), "Bridge Instrumentation and Structural Monitoring," ***European Bridge Conference 2022*** (Abstract Accepted), June 2022.
- Jayaseelan, H., and Russell, B.W., **"*Early Age Deflections in Composite Bridge Girders with Concrete Slabs,*"** Research in Progress, ACI Fall Convention, October 2018, Las Vegas, NV.
- Jayaseelan, H. (Presenter) and Russell, B., **"*Early Age Deflections in Steel Girder Bridges made composite with Concrete Slab,*"** Southern Plains Transportation Center, Summer Symposium. Oklahoma City, OK., August 2018.
- Russell, B.W., Acheli, A.E., and Filip, C.J. (2021), "*Structural Monitoring of PC Beams in the PC Bridge Over N. Canadian River and Recommendations for Improving Designs."* Oklahoma Transportation Research Day, Poster Presentation, October 2021.
- Russell, B.W. (Invited Presenter), Acheli, A.E., Filip, C.J. and Cochran, D. (2021), *"Structural Monitoring of PC Beams in the SH 4 Bridge over the N. Canadian River and Recommendations for Improving Designs."* Southern Plains Transportation Center Webinar, July 2021. (Online).
- Cochran, D., Jayaseelan, H. and Russell, B.W., *"Investigation of Effects of Concrete Creep Due to Tensile and Compressive Loadings."* Poster Presentation, Oklahoma Transportation Research Day, November 2019.
- Jayaseelan, H. (Presenter), Cochran, D., Acheli, A., and Russell, B.W., *"Impact of Thermal Loading on the Performance of Steel-Concrete Composite Bridge Girders"*, Poster Presentation, Oklahoma Transportation Research Day, October 2018.
- Jayaseelan, H. (Presenter) and Russell, B.W., *"Investigation of Ride Quality and Long-Term Performance in Rehabilitated Steel Bridges Made Composite with Concrete Deck Slabs",* Poster Presentation, Oklahoma Transportation Research Day, October 2017.
- Russell, B.W. (Presenter), Belcher, K., Abdelmeguid, I., and Jayaseelan, H., *"Shrinkage Induced Deformations in Steel Bridges Made Composite with Concrete Deck Slabs",* Oklahoma Transportation Research Day, October 2015.
- Belcher, K., Abdelmeguid, I., Jayaseelan, H. and Russell, B. *"Shrinkage Induced Deformations in Steel Bridges Made Composite with Concrete Deck Slabs (Poster Presentation)",* Poster Presentation, Oklahoma Transportation Research Day, October 2015.

3. Forensic Investigation of Known Bridges

In 2012, as an early part of the research program, forensic investigations were performed on three recently rehabilitated bridges. The three bridges selected were: 1) SH 86 over Stillwater Creek in Payne Co.; 2) SH 14 over Eagle Chief Creek, Bridge "A" in Woods Co., and 3) US 281 over Mule Creek in Woods Co. Of these bridges, SH 86 and SH 14 were reported to have ride issues relatively soon after construction was completed. The bridges at SH 86 and SH 14 had decks that were cast with screed elevations set at the edge of the concrete deck slabs, at locations cantilevered 3 ft. or more from the C.L. of the outside girder. In contrast, screeds for the deck slabs on the US 281 were set directly atop the outside girders, and elevations outside of the screeds were set by hand float. All three of these bridges were thoroughly inspected.

3.1.   SH14 Over Eagle Chief Creek Bridge "A", Woods Co.

A photograph of the Eagle Chief Creek, Bridge "A" in Woods Co. is shown in **Error! Reference source not found.** looking south along the east side of the bridge. Site investigations were performed on September 18 and September 23 of 2014. The Woods Co. Bridge is 30 ft - 8 in. wide measured out-to-out (o/o) and supported by five girder lines with 3 ft - 4 in. cantilevered overhangs. The two end spans were at 40 ft - 9 in. and the two middle spans were 40 ft - 0 in. from center-to-center (c/c) of bearings.

The plans for the retrofit called for an 8 in. concrete deck slab with a super-elevation slope of 1%. Decks are supported by W24 x 94 Gr. 33, A7 steel girders, and shear studs were installed as part of the rehabilitation. The steel girders are spaced at 6 ft and constructed with steel diaphragms at the ends and mid span locations. Steel girders were supported by steel bearings, some of which act as pins and some which are constructed to act as rollers.

Figure 3.1. SH 14 Over Eagle Chief Creek, Bridge "A", Woods Co., Oklahoma. View lkg South

New slabs were cast in 2010 or 2011 atop existing steel girders. At the same time, some rehabilitation or reconstruction of abutments was also done. Immediately upon construction, the bridge was reported to have issues with ride quality. Field investigations were performed as part of this research effort. Inspection found that the concrete deck slabs were uniformly in good condition with minor cracking exhibited both top and bottom of the bridge deck. There was also evidence of repair and new detailing at the abutments. Bridge piers and pier caps, and bearing assemblies were found in good condition. Elevation measurements were taken to assess the

elevation changes within the driving lanes, and to also help determine causes for possible adverse beam deflections. In **Error! Reference source not found.**, the girders possess a visible sag, perhaps in place from earlier construction or perhaps developed over the period of long service prior to the retrofit. Elevations at the bottoms of the beams were measured, and these confirmed that the bottoms of the beams have lower elevations at midspan than at supports.

Elevation measurements were made with traditional surveying equipment including an engineering level and leveling rod marked in hundredths of a foot. Elevations were measured at the bottoms of steel girders, at the bottom of concrete decks and atop the roadway surface (at the top of the concrete deck). Elevations were referenced to the T.O. of the east edge of the South Bridge Abutment (Abutment #1). **Error! Reference source not found.** reports roadway elevations at the top of the concrete deck. Elevations at the northbound and southbound shoulders were measured immediately outside of the lane stripe. Centerline (CL) elevations at or near the center line striping. CL Elevations vary from 3.51 to 3.58 ft. The "crown height" reported in the table measures the elevation at CL compared to the average elevation of the two shoulders. "DG" indicates locations where diamond grinding was visible in the traffic lanes, so it is possible and even probable that reported problems with ride were corrected somewhat with diamond grinding.

Table 3.1 Roadway Elevations at the Top of Concrete Driving Surface of SH 14 Bridge

	Feet from South Joint	ELEV @ N-Bound Shoulder	Crown (ft)	ELEV @ CL		ELEV @ S-Bound Shoulder
Span 1	0	3.46	0.08	3.51	DG	3.40
Span 1	10	3.42	0.11	3.52	DG	3.40
Span 1	20	3.41	0.12	3.54		3.42
Span 1	30	3.40	0.12	3.53		3.42
Span 1	40	3.47	0.11	3.57		3.45
Span 2	40	3.46	0.10	3.55		3.44
Span 2	50	3.38	0.11	3.51		3.41
Span 2	60	3.39	0.11	3.51	DG	3.41
Span 2	70	3.40	0.13	3.53	DG	3.41
Span 2	80	3.47	0.12	3.57	DG	3.44
Span 3	80	3.48	0.11	3.57	DG	3.44
Span 3	90	3.47	0.11	3.56	DG	3.43
Span 3	100	3.44	0.11	3.55		3.43
Span 3	110	3.45	0.11	3.56		3.44
Span 3	120	3.49	0.10	3.59		3.48
Span 4	120	3.50	0.09	3.58		3.48
Span 4	130	3.46	0.13	3.58		3.45
Span 4	140	3.46	0.13	3.58		3.45
Span 4	150	3.47	0.12	3.58	DG	3.45
Span 4	160	3.52	0.08	3.57	DG	3.45

	Feet from South Joint	ELEV @ N-Bound Shoulder	Crown (ft)	ELEV @ CL		ELEV @ S-Bound Shoulder
N. Approach	160	3.52		3.57		3.45
N. Approach	170	3.43		3.50		3.38
N. Approach	180	3.32		3.41		3.27

Notes:
1. Elevations measured relative to the Top of Abutment #1 (SE Corner Abutment).
2. N-Bound Shoulder and CL Elevations were measured from Instrument Location SE of the bridge deck. S. Bound Shoulder Elevations were measured from Instrument Location NW of bridge deck.
3. "ELEV @ CL reports the elevations at the roadway centerline.
4. "DG" indicates where diamond grinding was visible. Crown Height is the ELEV @CL minus the average ELEV @ the shoulders.

The values reported in **Error! Reference source not found.** are also shown in the chart in **Error! Reference source not found.**. **Error! Reference source not found.** shows the elevations of the SH 14 bridge at the centerline and at the North and South bound shoulders. The elevations were graphed from the South end of the bridge to the North end. From **Error! Reference source not found.**, we can see that Span #2 (40 ft. to 80 ft.) has the worst elevation "dip", about 5/8 in. at CL, but with as much as 1.0 in. dip at the South-bound shoulder. Diamond grinding has apparently relieved some of the ride-ability issues since the construction was completed.
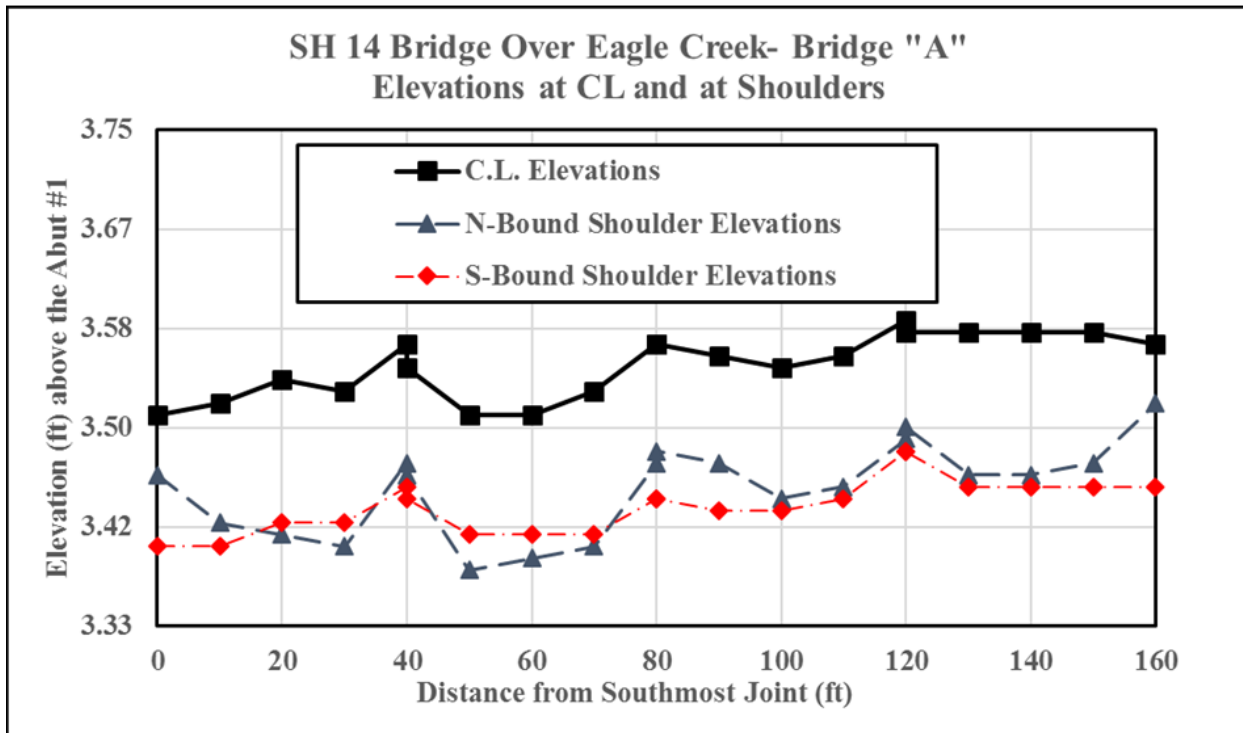
Figure 3.2 Elevations of the Bridge Deck, C.L. and Shoulders (ft. above the S. Abutment)

Figure 3.2 charts the elevations of the Bridge Deck at Centerline (C.L.), and at both shoulders. Elevations are shown in feet (ft) above the South Abutment. The chart shows the "dips" that occur in the middle portions of each of the three spans, and also shows that the "dips" for each span are evident at the Roadway C.L. where Span 2 "dips" from 3.57 ft. to 3.51 ft., or 6 in. The charts in Figure 3.2 also shows that the "dips" occur at both the N-Bound Shoulder and the S-Bound Shoulder. Figure 3.2 essentially shows the "picture" of the data found in Table 3.1

The elevations shown in both **Error! Reference source not found.**. and **Error! Reference source not found.** also indicate a super-elevation consistent with the "1 percent slope" prescribed on the construction drawings. A 1 percent slope in 12 ft. of lane width correlates to a 0.12 ft. elevation change, which is equivalent to 1.5 in.

Error! Reference source not found. reports the roadway elevations recorded at the bottom of the deck slab. The readings were recorded at locations "outside" the girders, and at locations approximately mid-way between the steel girders. Altogether, for each station measured in "Distance from the Joint at Abutment #1," six direct elevation measurements were made. The reported "Average Elevation at Bridge CL" is computed from the average of the two nearest elevations.

Table 3.2 Elevations recorded at the Bottom of the Bridge Deck (ft. above the S. Abutment)

	Dist. fr. Joint at Abut #1 (ft)	Outside East Girder (#1)	Between #1 and #2 Girders	Between #2 and #3 Girders	Average Elev @ Bridge CL	Between #3 and #4 Girders	Between #4 and #5 Girders	Outside West Girder (#5)
Span 1	2	2.72	2.80	2.85	2.84	2.84	2.79	2.74
Span 1	20	2.78	2.78	2.83	2.83	2.82	2.80	2.75
Span 1	38	2.79	2.80	2.86	2.86	2.87	2.81	2.80
Span 2	42	2.77	2.80	2.88	2.87	2.87	2.83	2.78
Span 2	60	2.79	2.78	2.87	2.86	2.85	2.79	2.74
Span 2	78	2.79	2.93	2.93	2.94	2.95	2.91	2.87
Span 3	82	2.80	2.84	2.87	2.87	2.88	2.82	2.80
Span 3	100	2.79	2.79	2.84	2.85	2.87	2.82	2.76
Span 3	118	2.80	2.82	2.87	2.87	2.88	2.86	2.82
Span 4	122	2.80	2.84	2.87	2.87	2.88	2.82	2.80
Span 4	140	2.79	2.79	2.84	2.85	2.87	2.82	2.76
Span 4	**158**	2.80	2.82	2.87	2.87	2.88	2.86	2.82

Notes:
1. Elevations measured relative to the T.O. Abutment #1 (SE corner abutment).
2. Readings recorded approximately mid-way between the steel girders, or immediately outside the exterior girder.

The elevations measured and reported in **Error! Reference source not found.** and **Error! Reference source not found.** are compared to one another in **Error! Reference source not found.**, where the slab thicknesses are reported. Slab thicknesses are computed from the measured elevations and represent the difference between the elevations at the bottom of the slab to the elevation of the driving surface. Red numbers in **Error! Reference source not**

found. indicate measurements where the deck slab thickness is less than the required 8 in. Again, "DG" denotes areas where diamond grinding was performed in the traffic lanes. It is also noted and reported that the diamond grinding visibly reduced the depth of the tines that were likely installed with finishing.

Table 3.3 Slab Thickness of the SH 14 Bridge Deck (ft.), Computed from Elevation Readings

	Feet from South Joint	N-Bound Shoulder	CL		S-Bound Shoulder
Span 1	0	0.74	0.67	DG	**0.66**
Span 1	10	0.67	0.69	DG	**0.66**
Span 1	20	**0.63**	0.71		0.67
Span 1	30	**0.61**	0.69		**0.65**
Span 1	40	0.68	0.71		**0.65**
Span 2	40	0.69	0.68		**0.66**
Span 2	50	0.60	0.65		**0.65**
Span 2	60	0.60	0.65	DG	0.67
Span 2	**70**	0.61	0.63	DG	**0.61**
Span 2	80	0.68	0.63	DG	**0.58**
Span 3	80	0.68	0.70	DG	**0.65**
Span 3	90	0.67	0.70	DG	**0.66**
Span 3	100	**0.65**	0.70		0.68
Span 3	110	**0.66**	0.70		**0.66**
Span 3	120	0.69	0.72		0.67
Span 4	120	0.70	0.70		0.69
Span 4	130	**0.66**	0.72		0.67
Span 4	140	0.67	0.74		0.69
Span 4	150	0.68	0.73	DG	0.67
Span 4	**160**	0.72	0.70	DG	**0.64**

Pre-existing core holes were discovered in Span #2 and Span #4 at the center of the northbound driving lane. Figure 3.3 shows photographs of measurements made on deck thickness at two separate holes found pre-existing in the deck slab. Thicknesses at the core holes were measured at approximately 7.25 in. in Span #2 and approximately 8.25 in. in Span #4. The measured thicknesses match the slab thicknesses computed in **Error! Reference**

source not found. These observations confirm that the method for determining slab thickness from measured surface elevations is an accurate means to obtain forensic data. The slab thicknesses measured using the engineering level were consistent with the depth of the slab measured from pre-existing core holes in the deck in Spans #2 and #4. The cores were from unknown origin.
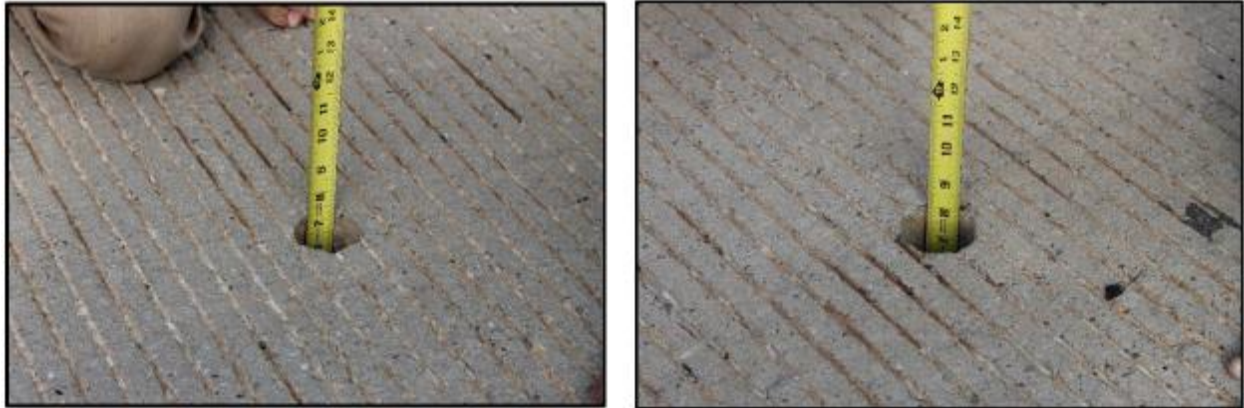
Figure 3.3 Direct Measurement of Bridge Deck Slab Thickness at Pre-Existing Core Holes in Span #2 (left) and Span #4 (right)

3.2. SH 86 Bridge over Stillwater Creek, Payne Co.

The SH 86 Bridge was reported by witness accounts as having ride-ability issues immediately after construction. Interviews were conducted with both the Contractor's representative and the ODOT Field Engineer. **Error! Reference source not found.** shows a photograph of the SH 86 Bridge looking southwest and spanning Stillwater Creek.

Figure 3.4 SH 86 over Stillwater Creek, Payne Co., Oklahoma, View Lkg SW

The bridge is located at the westernmost reaches of Lake Carl Blackwell, which is wholly located on property owned by the Oklahoma A&M University system. This land was part of the original "Land Grant" made in accordance with the Morrill Act that instituted the Land Grant Universities in numerous states. This bridge has three spans, each approximately 60 ft in length. During or about 2011, the bridge was rehabilitated by casting a new concrete deck atop existing steel bridge girders.

Table 3.4 Elevations at Top of Concrete Driving Surface (ft. above the N. Abutment), SH 86 Bridge over Stillwater Creek, Payne Co., Oklahoma

	Feet (ft) from the Joint at Abut. #1	East Edge (Against Guardrail)	Just Outside N. Bound Lane Marker	CL	Just Outside S. Bound Lane Marker	West Edge (Against Guardrail)
North Span	0	5.38	5.33	5.24	5.53	5.58
North Span	10	5.45	5.40	5.31	5.60	5.65
North Span	20	5.51	5.44	5.33	5.62	5.66
North Span	30	5.53	5.46	5.36	5.62	5.67

	Feet (ft) from the Joint at Abut. #1	East Edge (Against Guardrail)	Just Outside N. Bound Lane Marker	CL	Just Outside S. Bound Lane Marker	West Edge (Against Guardrail)
North Span	40	5.50	5.44	5.33	5.60	5.65
North Span	50	5.47	5.40	5.29	5.56	5.65
North Span	60	5.39	5.32	5.29	5.51	5.57
Middle Span	60	5.41	5.33	5.29	5.53	5.60
Middle Span	**70**	5.45	5.38	5.27	5.58	5.67
Middle Span	80	5.50	5.41	5.30	5.60	5.66
Middle Span	90	5.50	5.42	5.32	5.60	5.67
Middle Span	100	5.50	5.40	5.30	5.60	5.67
Middle Span	110	5.47	5.37	5.27	5.55	5.67
Middle Span	120	5.37	5.31	5.23	5.50	5.56
South Span	120	5.39	5.31	5.23	5.51	5.58
South Span	130	5.46	5.36	5.25	5.55	5.65
South Span	140	5.47	5.39	5.27	5.58	5.65
South Span	150	5.46	5.38	5.29	5.59	5.67
South Span	160	5.45	5.37	5.27	5.57	5.66
South Span	170	5.42	5.35	5.25	5.55	5.60
South Span	**180**	5.33	5.29	5.19	5.48	5.52
S. Approach	180	5.32	5.28	5.18	5.48	5.52

	Feet (ft) from the Joint at Abut. #1	East Edge (Against Guardrail)	Just Outside N. Bound Lane Marker	CL	Just Outside S. Bound Lane Marker	West Edge (Against Guardrail)
S. Approach	170	5.34	5.29	5.20	5.49	5.53
S. Approach	180	5.39	5.35	5.23	5.52	5.54

Notes:

1. Elev. 0.00 is taken at the East corner of the North Abutment.

2. CL elevations were taken at or near the centerline striping.

3. The outside lane markers are 12 ft from the C.L.

4. The inside dimension from guardrail to the CL is 15'-6.

5. Prescribed super-elevation is 1.0% sloping outward from the C.L.

The forensic investigation was performed in May 2014 and in September 2014. Elevations of the driving surfaces were taken on all three spans relative to the elevation of the north abutment. These elevations are reported in **Error! Reference source not found.** Elevations were measured at 10 ft. intervals at the guardrails, at the outside lane marker and at roadway centerlines. Generally, the topside elevations show a clear pattern where the riding surfaces "dip" approximately 0.75 to 1.75 in. near the mid-spans of all three spans. At the centerline, the measured elevations "dip" 1.3 in. in north span, ¾ in. in the center span and 1.02 in. in the south span. Elevation "dips" at the outside lane markers are more severe and vary from 1.00 in. to 1.75 in. Elevations were measured at the outside lane marker for both Northbound and Southbound Lanes. East and West Guardrail elevations were measured just inside the guardrail. All the measurements were taken to the top of the concrete deck slab.

Error! Reference source not found. clearly shows the patterned changes in roadway elevations where the roadways "dip" approximately 0.75 in. to 1.3 in. at midspan. **Error! Reference source not found.** also shows elevation changes at the outside lane markers and at the guardrails. The figure shows a clear pattern of lower elevations at the mid-regions of the spans and "humps" at the pier supports. These elevation changes are noticeable to drivers operating at highway speeds, and likely cause concerns for safety. **Error! Reference source not found.** reports elevations measured to the bottoms of the deck slab. Elevations on the bottom of the bridge deck were taken only on the northern most span as the other two spans were inaccessible due to water from the lake. Measurements between girders were made at mid-distance between beams. Two measurements were made outside of the outside girders. One measurement was made immediately adjacent to the outside girder at approximately 13 ft – 4 in. from C.L. The measurement shown as "East (or West) Deck Edge" was made at the edge of the deck slab, taken approximately 16 ft – 6 in. from the C.L. of the bridge deck.
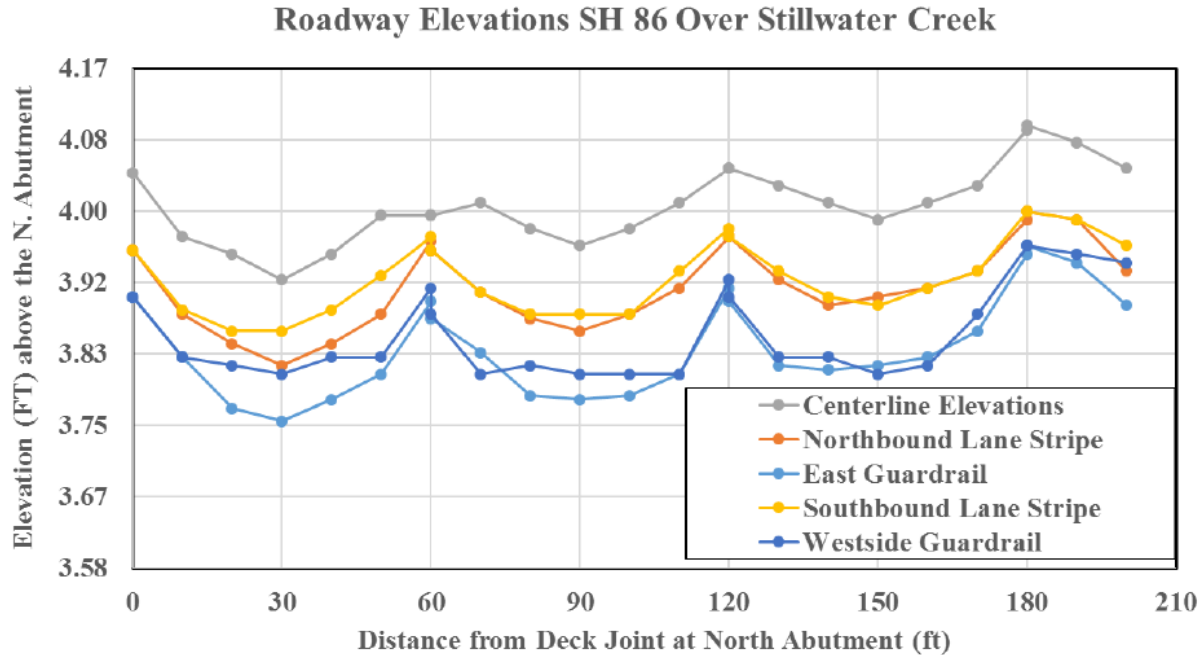
Figure 3.5 Elevations of Top of Concrete Driving Surfaces, SH 86 Bridge over Stillwater Creek, Payne Co. Oklahoma

Stay-in-place forms were used on the SH 86 bridge whereas they were not used on the other two bridges that were inspected. The stay-in-place forms are made from galvanized metal decking. The decking itself is variegated; the depth of the variegation is 1.25 in. Elevations at the bottom of the slab were measured inside the top of the variegation, so elevations were measured at the thinnest part of the slab. Elevations measured outside of the steel girders were made directly to the bottom of concrete, which was exposed and did not feature stay-in-place forms. The concrete decks slab profile in **Error! Reference source not found.** shows the slab elevations at the midspan of the north span of the bridge. The elevation at the top of the slab is shown as well as the elevations at the bottom of the slab. Elevations of the top of the slab correspond to these values reported in **Error! Reference source not found.** at "North Span, 30 ft": East Edge, 3.76; N. Bound Lane Marker, 3.82; C.L., 3.92; S. Bound Lane Marker, 3.86; and West Edge, 3.81. Note that a 1.0 percent slope was required for super-elevation. The actual super elevation slopes are reported in **Error! Reference source not found.**, and it is noted that measured elevations indicate super-elevations of 1.03 percent on the northbound lane and 0.81 percent on the southbound lane.

Table 3.5 Elevations recorded at the Bottom of the Bridge Deck Slab (ft. above the N. Abutment), SH 86 Bridge over Stillwater Creek, Payne Co.

		West Deck Edge	O/S West	#7/#6	#6/#5	#5/#4(CL)	#4(CL)/ #3	#3/#2	#2/#1	O/S East	Deck Edge East	Dist. Fr. S.
@Face of N.Abut.		3.158	3.226	3.268	3.299	3.341	3.367	3.346	3.263	3.231	3.179	0
	10'-0	3.127	3.231	3.226	3.299	3.367	3.356	3.315	3.231	3.190	3.106	10
@Diaphra gm	20'-0	2.849	3.010	3.057	3.109	3.341	3.346	3.294	3.231	3.200	3.080	20

		West Deck Edge	O/S West	#7/#6	#6/#5	#5/#4(CL)	#4(CL)/#3	#3/#2	#2/#1	O/S East	Deck Edge East	Dist. Fr. S.
@Midspan	30'-0	3.06	3.20	3.23	3.29	3.37	3.33	3.30	3.22	3.16	3.03	30
@Diaphragm	40'-0	3.10	3.20	3.23	3.30	3.34	3.34	3.31	3.24	3.19	3.04	40
	50'-0	3.06	3.19	3.25	3.30	3.34	3.33	3.32	3.25	3.22	3.10	50
@Face of S. Pier		3.13	3.24	3.29	3.34	3.37	3.34	3.32	3.28	3.23	3.14	60
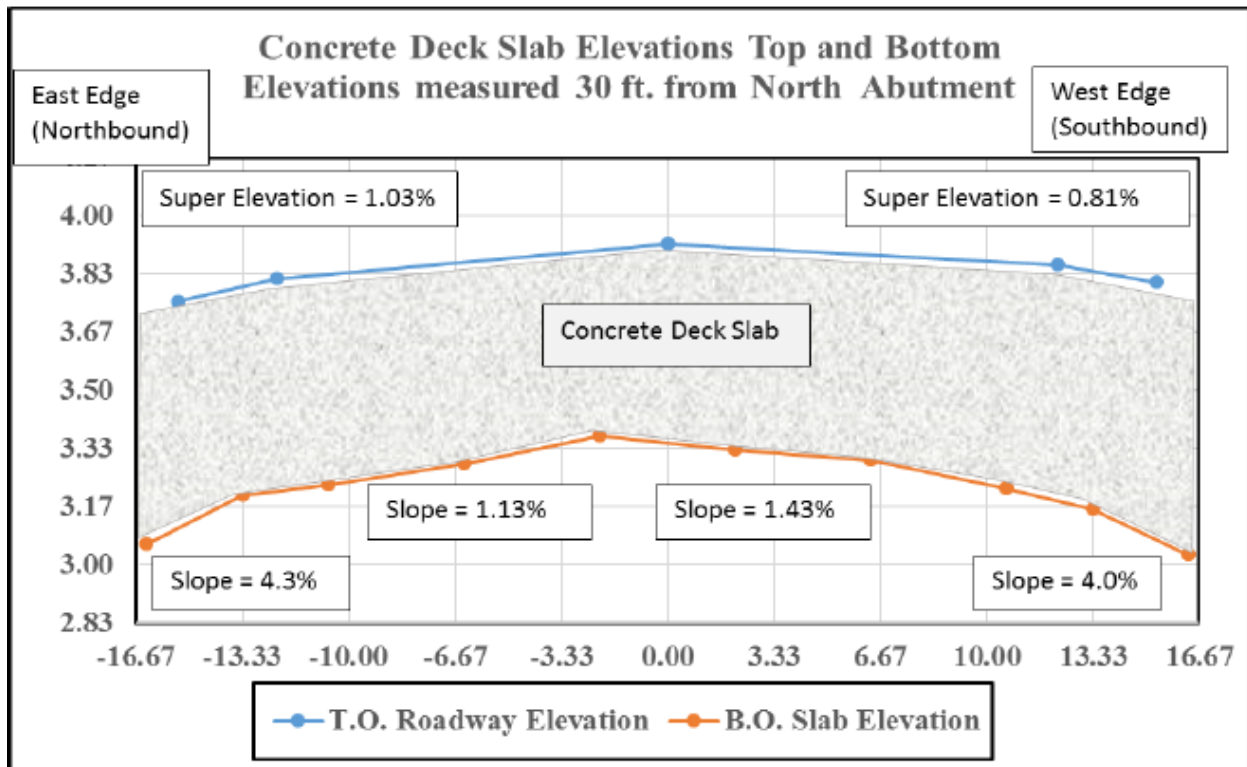
Figure 3.6 Deck Slab Profile of SH 86 Bridge, @ Mid-span of the North Span, based on Elevation Readings (0.00 = T.O. N. Abutment)

Error! Reference source not found. also charts the elevations measured at the B.O. of the concrete deck that correspond to values reported in **Error! Reference source not found.** at 30 ft – 0 in. from the North Abutment. Those elevations in **Error! Reference source not found.** are reported as: 3.06, 3.20, 3.23, 3.29, 3.37, 3.33, 3.30, 3.22, 3.16 and 3.03 feet. The concrete bridge deck resides within the space between the T.O. Deck and the B.O Deck, and the difference between the two sets of elevations provides a direct measure of the bridge deck thickness.

Error! Reference source not found. also shows the slopes on the bottom side of the cast deck slab. Slopes measured from Roadway C.L. to the outside girders are 1.13 percent and 1.43 percent on the Southbound and Northbound sides, respectively. More importantly, **Error!**

Reference source not found. reports larger slopes measured from the outside girder to the outside edge. On the Northbound side the slope is 4.3% and on the Southbound side the slope is 4.0 percent. The slopes at the bottom of the slabs are more severe, or steeper, near the edges of the slab. These regions corresponds to portions of the deck slab formwork that cantilevered from the outside girder to the edge of the slab. These intensified slopes indicate unusually large deflections of the bracing and formwork outside of the outside girder. This is significant because the screeds that set elevation controls for the finished elevations of the deck slabs are set directly upon the formwork at the outside edge of the deck slab. The data clearly show that the formwork is inadequately braced, which results in steeper slopes on the bottom of the bridge deck. In turns, these deformations are the direct cause for poor elevation control over the mid-regions of the bridge spans. Not only is poor elevation control the cause for poor ride quality, but it is also the cause for thin bridge decks which will negatively impact service life.

Slab thicknesses on the North Span of the SH 86 Bridge are computed and shown in **Error! Reference source not found.** From the tabulation, one can see that bridge deck thickness are significantly less than 8 in. as required by the design, and that some of the thicknesses are less than 7 in. The thinnest measurement for the bridge deck occurs at the C.L. at midspan of the North Span, 0.57 ft, which corresponds to 6-7/8 in. The intent of the Bridge Engineer is that the deck slabs should be 8 in. thick. The thickness of the slab is required for flexural and shear strength of the deck itself, so clearly the thin decks result in understrength deck slabs. Additionally, the thickness provides cover for reinforcing steel, so thinner decks are likely to adversely affect the durability of these bridges somewhere in the future. Additionally, thin decks reduce the dead load of the bridge superstructure and potentially make the bride more vulnerable to vibration and fatigue from repeated loads. So, the data show that not only are the road way elevations responsible for poor ride quality, the data also show that bridge decks are being cast at significantly thinner depths than required for design.

Table 3.6 Slab Thickness (ft) of the SH 86 Bridge, North Span Computed from Measured Elevations

Distnace from N. Bridge Joint	East Edge (Against Guardrail)	Just Outside N. Bound Lane Marker	CL	Just Outside S. Bound Lane Marker	West Edge (Against Guardrail)
0	0.72	0.71	0.69	0.71	0.70
10	0.67	0.65	0.61	0.67	0.70
20	0.87	0.81	0.61	0.64	0.70
30	0.65	0.60	0.57	0.67	0.74
40	0.65	0.63	0.61	0.67	0.74
50	0.71	0.66	0.66	0.69	0.69
60	0.73	0.70	0.64	0.71	0.74

Notes: Slab thickness is shown in feet (ft). The specified thickness for the deck slabs is 8 in. All of the slab thicknesses shown in the table that are less than 0.67 ft. are thicknesses less than the required amount. Thin deck slab is most common at the Roadway CL and at locations near the midspan of the north span. The least thickness dimension of 0.57 ft. (7.0 in.) is located at midspan at the Roadway CL.

Altogether the forensic evidence indicates that problems with ride-ability resulted principally from construction related incidences. The evidence strongly suggests that large and localized deflections occurred within formwork that supported the cantilevered portions of the bridge deck slab. Furthermore, these localized deflections also produced larger than expected deflections of the screeds that set elevation controls for the deck slabs, and in turn resulted in finished concrete slabs with elevations at midspan that are lower than the elevations at the piers and abutments. This also caused thin bridge decks as shown in our forensic evidence.

3.3.   US 281 over Spring Creek, Woods Co.

This bridge features three spans. Each span is approximately 30 ft - 0 in. in length. New concrete bridge decks were cast atop existing steel girders during the rehabilitation of the bridge. The bridge is located approximately 2.5 mi. south of the Oklahoma/Kansas state line, and north of Alva, Oklahoma. According to a witness account, screed rails for the new concrete decks were set atop the outside steel girders, and that the slab from the rail to the outside edge of the deck was screeded by hand. Figure 3.7 features the photograph of the bridge with a view looking northeast. Summer conditions promote brush and vegetation in this intermittent creek.

Figure 3.7 US 281 Bridge over Spring Creek, Woods Co., Oklahoma, View Lkg SW

Investigation of the concrete deck condition and elevations were performed. Elevations for this bridge were obtained at the top of the concrete deck at centerline, and at the north bound and south bound shoulders. Table 3.7 reports the roadway elevations of US 281 Over Mile Creek bridge. Interesting to this bridge, the centerline elevations vary no more than 1/8 in. for all three spans. Elevations are flat, first of all, but the physical measurement of centerline elevations revealed that the most variation that occurred was 0.01 ft., or 1/8 in. No diamond grinding has been done to the concrete surface.

Table 3.7: Roadway Elevations (ft.) above abutment, US 271 Over Spring Creek, Woods Co. OK.

	Dist. fr. Joint at Abut #1 (ft)	N-Bound Shoulder	Crown	CL	S-Bound Shldr
		3.53	0.18	3.68	3.47
S. Approach		3.50	0.18	3.67	3.48
		3.51	0.20	3.70	3.49
Span 1	0	3.51	0.19	3.69	3.49
Span 1	5	3.47	0.21	3.68	3.47
Span 1	10	3.44	0.23	3.68	3.46
Span 1	15	3.45	0.23	3.68	3.46
Span 1	20	3.48	0.20	3.68	3.48
Span 1	25	3.49	0.19	3.69	3.51

	Dist. fr. Joint at Abut #1 (ft)	N-Bound Shoulder	Crown	CL	S-Bound Shldr
Span 1	30	3.51	0.18	3.69	3.52
Span 2	30	3.50	0.19	3.69	3.51
Span 2	35	3.49	0.20	3.69	3.50
Span 2	40	3.49	0.21	3.69	3.47
Span 2	45	3.49	0.21	3.69	3.48
Span 2	50	3.48	0.21	3.69	3.48
Span 2	55	3.48	0.21	3.69	3.49
Span 2	60	3.48	0.20	3.68	3.48
Span 3	60	3.49	0.20	3.69	3.49
Span 3	65	3.48	0.21	3.70	3.50
Span 3	70	3.47	0.21	3.69	3.50
Span 3	75	3.47	0.21	3.69	3.50
Span 3	80	3.49	0.20	3.69	3.49
Span 3	85	3.51	0.19	3.70	3.51
Span 3	90	3.55	0.19	3.74	3.54

Table 3.8 reports the calculated slab thickness for span #3 of this bridge. It can be noted that the slab thickness is nearly 9 in. throughout span length. Furthermore, this bridge exhibits none of the problems of ride quality or thin construction of bridge decks that are exhibited in the other two bridges.

Table 3.8: Calculated Slab thicknesses (ft) for Span #3 for the US 281 Bridge over Spring Creek.

Dist. fr. Joint at Abut #1 (ft)	N-Bound Shoulder		CL		S-Bound Shldr
60	0.73		0.76		0.71
65	0.72		0.77		0.74
70	0.72		0.76		0.76
75	0.73		0.75		0.77
80	0.76		0.76		0.76
85	0.78		0.78		0.76
90	0.82		0.82		0.77

4. Laboratory Investigations:

4.1. Overhang Brackets Load Testing:

The bracing and formwork have proved to be one of the most important aspects of this project. Through this work, findings confirm the findings from forensic Investigation; that is that the problems in ride quality in rehabilitated steel girder bridges are the direct result of formwork and bracing that is supported inadequately. Further, that deflections occurring during construction of the concrete deck, most specifically the deflections that occur during the placement of the fresh concrete in the formwork and using typical screeding operations – are the principal causes for adverse ride quality.

Bridge decks generally include a cantilevered or overhanging portion that extends from the centerline of the exterior girder to the edge of the bridge deck. The cantilevered sections are normal, as it is logical for the concrete deck to extend beyond the C.L. of the outside girder. However, in rehabilitation of some bridge decks, the cantilevers are increased beyond original design in order to increase the overall width of the bridge.

The width of the overhang is typically limited to three or perhaps four feet to help balance load distributions between exterior and interior girders. During deck casting, the overhanging portion of the bridge deck is supported using temporary wooden formwork supported by steel brackets that are in turn attached to the exterior girders. Horizontal thrust from the brackets is usually applied against the web of the outside girders. These overhang brackets must be strong and stiff enough to transfer various construction loads to the bridge superstructures. Construction loads include supporting formwork, workers, construction equipment including the screeding machine, the screed rail, and fresh concrete. When large cantilevers are supported by relatively shallow girders, the effects of construction loads are increased by the geometry of the bracing. The proper design of bridge overhang bracket systems is critical to hold the dead weight of the fresh concrete, finishing screed and other construction loads during the time of deck pour.

The C-49 overhang bracket a product of Dayton Superior and one of the most versatile overhang brackets used by DOT bridge. It is widely use in both prestressed concrete girders and in steel girders composite with concrete deck slabs. The bracket is typically made of light gage steel pipe and channel sections. Steel hangers are placed on top flange of the steel girder and the overhang brackets are held in position via ½" coil rods and steel hook bolts. The bracket typically adjusts from a minimum depth of 30 into a maximum depth of 50 in. However, the ODOT standard drawings specify that the bottom leg of the braces on the cantilever forming should bear on the girder webs within 6 in. of the bottom flange of the steel girders. The standard drawings also specify that the formwork bracing should continue between the steel girders at intervals of 4 ft. or less where possible through skewed regions at the ends of the deck.

4.1.1. Full-Sized Prototype Bridge & Testing of Overhang Bracket Systems:

The research team constructed the prototype systems for testing the bracing systems for formwork and screeds in accordance with ODOT design standards and details shown on typical drawings. The prototype bridge in the Cooper Lab matches the steel superstructure of the SH14 Bridge over Eagle Chief Creek (Bridge "A") which features 40 ft. spans and W24x94 girder sections. The prototype for testing bracing systems also matches that of the prototype bridge that will be constructed. The prototype includes diaphragms at ends and mid spans of the 40 ft. span.

The prototype bridge spans 38 ft -10in. from center-to-center (c/c) of bearings with an 8 in. concrete deck supported by W24x94 Gr. 50 steel girders. The prototype bridge is cast with a 14 ft wide deck and supported by two girders at 6 ft spacing and 4 ft cantilevered overhangs. The Woods Co. Bridge has a width of 30ft. and 8 in. measured out-to-out (o/o) and supported by five girder lines with 3 ft- 4 in. cantilevered overhangs. The prototype bridge girders were named North and South girders with respect to their location at the Bert Cooper laboratory.

The temporary formwork for the laboratory prototype bridge was built with 2 x 4 lumber and ¾ in. thick plywood forms, supported with commercially available steel overhang brackets spaced at 4 ft. centers. The steel overhang brackets also match those commonly used by ODOT contractors for on-site construction of similar bridge decks. As with ODOT provided details, the overhang formwork was built to accommodate an additional walkway area on both sides of the girders. The bridge was installed with tension tie rods to connect the two girders at the top and 4 x 4 wooden blocking at the bottom of the webs between the girders in accordance to standard ODOT drawings. Typical standard details prescribed by ODOT for supporting the overhanging formwork are found in Fig. 4.10.
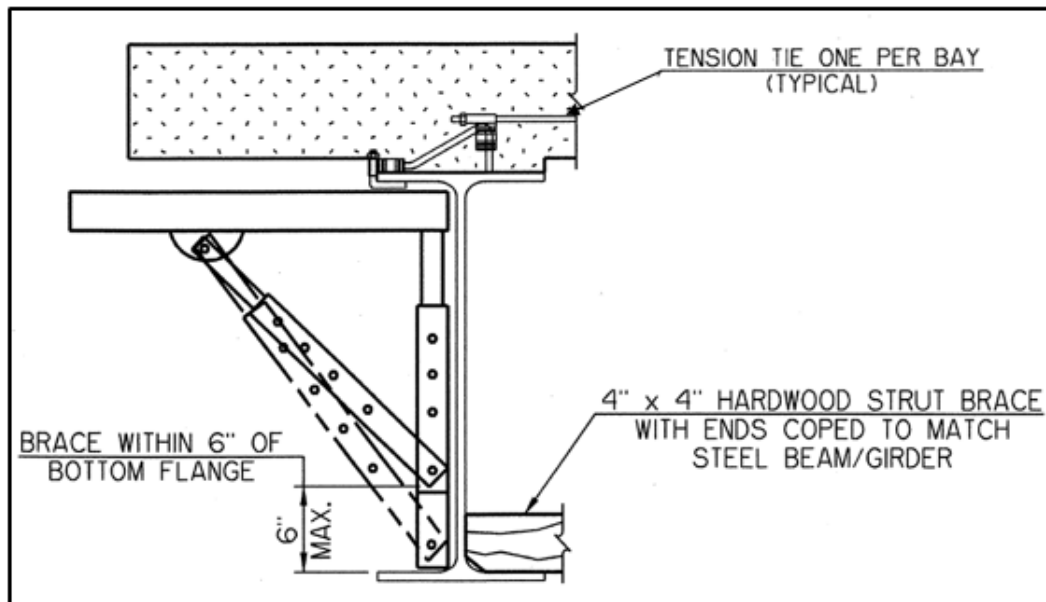
Figure 4.1: ODOT standard detail drawing for Bridge Deck Overhang Formwork Bracing (Dayton Superior Bridge Deck Handbook 2017)

The bracings that were employed for this research were bought from The Gamco Inc. The shop drawings of the bracing are shown in the following figure:
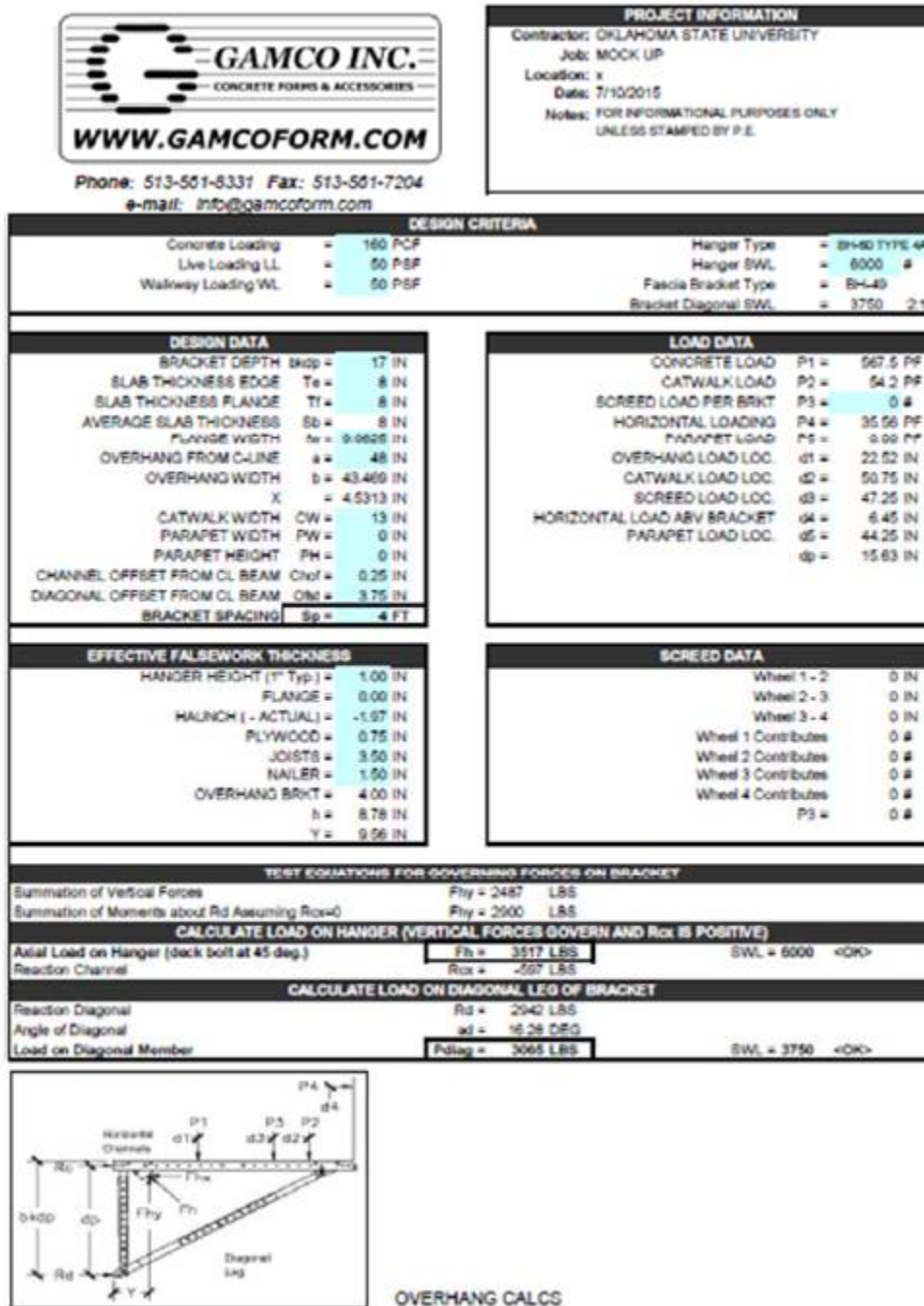
Figure 4.2: Bracing calculations provided by Gamco

The cantilever portions of the bracing were strengthened by adding wooden bracing to support the construction of the bridge deck on the full-sized prototype bridge beam. The bracing system

was further stiffened by adding diagonal wooden struts. In addition, the diagonal struts were shimmed to further stiffen the response of the bracing to temporary loads.

In Figure 4.3 below, the photograph shows the formwork with bracing that includes both the typical standard issue adjustable steel braces augmented with some wooden braces. Load vs. deflection measurements of the formwork were obtained with the five sacks of cement shown on the pallet that is supported by the bridge deck.

Prior to the deck cast the overhang formwork was tested for deflections at various locations on the bridge deck overhang and walkway areas. A simple load test was conducted using five 94 lbs. cement bags tallying a total load of 470 lbs. Figure 4.4. shows the cement bags load testing performed on mid span bracket located on the South side of Walkway Platform.

The brackets were loaded on top of the formwork at the bracing locations with increments of one cement bag at the time. Dial gages were installed to monitor the deflections in the overhang formwork and the steel girders. In addition, the lateral deflection of the steel girders due to the overhang loads were also monitored. The test was performed on both the walkway and deck locations for comparative study. For the walkway loading the overhang brackets were loaded at 5 ft. from the centerline of the girder on both sides. Both the North and South areas of the overhang formwork were loaded at mid-span bracket (about 9 ft- 5 in. from the end support), end bracket close to the East and West supports and at one quarter point bracket locations (about 4 ft- 8 in. from end support). The spacing of the overhang brackets was not varied during the time of testing. The continuity between the formwork panels and 2x4 framing was maintained and often extended on either sides of formwork panel joints.

Figure 4.3: Formwork being prepared for casting the bridge deck on the prototype bridge

Figure 4.4: Cement sacks are being used to provide eccentric loading to the formwork and bracing systems in order to measure the load effects on temporary structures.

The table and figures below provide details and results from load testing performed to test the bracing and formwork for deflections.

Table 4.1 reports the vertical deflections of the overhang formwork and girders and lateral deflection of the girders for each load positions and various bracket locations along the North and South sides of the formwork. From results it is observed that the deflection of the overhang formwork varies from 0.65 in. to 1.2 in. recorded at the edge of the walkway loading. Further, measured deflections varied significantly depending on the location of the applied loading. It can also be clearly observed that the end brackets deflected the most when loaded close to the East and West end supports of the girders. The tests were repeated with and without the 4 x4 wooden blocking at the bottom of the girders and tension ties that connect the two girders at the top. The results showed no big difference in the deflection of the brackets. In other words, the wooden blocking and the ties made very little if any difference in measured formwork deflections. The steel girders deflected to a maximum of 0.023 in. and continued to rotate and deflect as a result of the deflection of the brackets.

The steel girders have shown a maximum girder rotation of about 0.0017 radians and 0.0015 radians when loaded at the midspan bracket location of the North and South sides respectively. The results show that the steel girders along with the brackets and the tie beam act as one single system.

23

Table 4.1: Results of Bracing Load test without additional wooden bracing

Load Position	Bracket Location	Formwork Deflection (in.) at Load Point	North Girder Deflection at Midspan (in.)	South Girder Deflection at Midspan (in.)	Girder Rotation (rad)
North Edge Formwork	East End	0.863	0.002	-0.005	-
North Edge Formwork	East Quarter	0.958	0.011	-0.007	-
North Edge Formwork	Mid-span	0.704	0.013	-0.012	0.0017
North Edge Formwork	West Quarter	0.690	0.014	-0.011	-
North Edge Formwork	West End	1.206	0.003	-0.002	-
South Edge Formwork	East End	0.764	-0.006	0.001	-
South Edge Formwork	East Quarter	0.685	-0.005	0.014	-
South Edge Formwork	Mid-span	0.652	-0.006	0.012	0.0015
South Edge Formwork	West Quarter	0.721	-0.006	0.011	-
South Edge Formwork	West End	0.750	-0.003	0.001	-

Notes: Positive values indicate downward deflections and Negative values indicate upward deflections

Table 4.2: Results of Bracing Load test with additional wooden bracing

Load Position	Bracket Location	Formwork Deflection (in.) at Load Point	North Girder Deflection at Midspan (in.)	South Girder Deflection at Midspan (in.)	Girder Rotation (rad)
North Edge Formwork	East End	0.149	0.007	-0.003	0.001
North Edge Formwork	East Quarter	0.111	0.013	-0.004	0.004

Load Position	Bracket Location	Formwork Deflection (in.) at Load Point	North Girder Deflection at Midspan (in.)	South Girder Deflection at Midspan (in.)	Girder Rotation (rad)
North Edge Formwork	Mid-span	0.116	0.016	-0.005	0.001
North Edge Formwork	West Quarter	0.124	0.013	-0.004	0.03
North Edge Formwork	West End	0.085	0.007	0.002	0.0004
South Edge Formwork	East End	0.09	-0.005	0.005	0.0001
South Edge Formwork	East Quarter	0.128	-0.004	0.016	0.006
South Edge Formwork	Mid-span	0.121	-0.004	0.009	0.001
South Edge Formwork	West Quarter	0.141	-0.004	0.013	0.005
South Edge Formwork	West End	0.102	-0.004	0.005	0.001

Positive values indicate downward deflections and Negative values indicate upward deflections

Figure 4.5: Bracing of formwork for the cantilevers. Additional bracing shims were added to help reduce construction deflections.

From Notes: Positive values indicate downward deflections and Negative values indicate upward deflections

Table 4.2, it is observed that the maximum overhang bracket deflections are reduced to about 0.15 inches. This corresponds to about 88% reduction in the deflection of the overhang bracing system when additional support bracing is provided to stiffen the bracing system. The end bracing is found to deflect more than the others due to the absence of adjacent bracing to share the load. From tabulated results the recorded girder rotations are higher (0.006 radians) at the quarter bracing loading point when compared to the mid-span and the end bracket loading. This is due to the presence of rigid steel diaphragms at the end and mid span locations. Comparing the twisting of the girder at the mid-span location with the diaphragms and the quarter bracing at the end without the diaphragms, the twisting is almost five times more the location with no diaphragms. We can also observe that the twisting due to lateral deflection of the girder due to the loading at the mid and end span bracing is much less. This indicates that the presence of the rigid diaphragms prevents the twisting of the girder at the ends and at the midspan.

4.1.2. Discussion:

The results from forensic investigations performed on three field bridges provide strong evidence that unwanted deflections in rehabilitated steel-girder bridges are caused principally by poorly braced or poorly supported formwork. Two of the three bridges had elevation screeds set at the edge of the slabs at the far edges of the cantilevers. One of the three bridges had elevation screeds atop the C.L. of the exterior bridge beam. Measured elevations above and below deck slabs in the SH 86 Bridge show that the out slopes measured on the underside of the deck slabs increased dramatically in the cantilevered portions of the deck slab.

The results from laboratory investigations confirmed the findings of the forensic examinations. Load testing performed on the C-49 brackets clearly indicates that these brackets lack sufficient stiffness to support the overhang lengths of the bridges built with shorter girder depths. This provides direct evidence that the bracing and formwork that supported the weight of fresh concrete at the cantilever sections of the overhang, as well as construction activities, was insufficient to resist loading without adverse deflections. As the weight of fresh concrete plus the weight of finishing and screed machines was applied to formwork, the bracing deformed, and the formwork deflected causing permanent downward cast to the concrete surfaces.

The findings from this report indicate that the bracing systems detailed on ODOT's drawings and used by ODOT contractors are wholly insufficient to support the weight of the fresh concrete during slab casting. Moreover, when the weight of the fresh concrete is combined with the live load weights from the screed, other construction equipment, and workers, the deflection of the formwork and bracing can be excessive. An additional consequence is that thin decks were discovered near mid-spans of several structures. These are the most likely causes of adverse ride quality in newly built or rehabilitated bridge. These adverse outcomes are found to be a direct result of errors in both design and construction. Improved construction practices that place responsibility for elevation control on the contractor are highly recommended. ODOT should include performance criteria for the construction contracts that include a pay factor for roadway elevation control.

4.2. Full-Size Prototype Beam Instrumentation

This section of the report focuses on deflections and deformations that occur at early ages in newly rehabilitated bridges made from steel girders and composite concrete deck slabs. The research program responds to problems with elevation control and subsequent ride quality problems exhibited in newly constructed or newly rehabilitated steel girder bridges built with composite with concrete decks.

A full-sized prototype bridge was built at the Bert Cooper Engineering Laboratory. The bridge was constructed to replicate the Eagle Chief Creek Bridge "A" on SH 14 in Woods Co., Oklahoma (Figure 4.6). The Woods Co. bridge is shown in, and the full-sized prototype at the Cooper Lab is shown in Figure 4.7 . Both bridges span 40 ft from center-to-center (c/c) of bearings with 203 mm concrete decks supported by W24 × 94, ASTM A572 Grade 50 steel girders. The Woods Co. Bridge is 30'-8 wide measured out-to-out (o/o) and supported by five girder lines with 3'-8 cantilevered overhangs. The prototype bridge at the Cooper Lab has a deck 14 ft wide supported by two girders with 4 ft. cantilevered overhangs.

Figure 4.6: Eagle Chief Creek Bridge "A" on State Highway 14, Woods Co, OK. View looking North

Figure 4.7: Full-sized prototype at the Bert Cooper Engineering Laboratory at Oklahoma State University
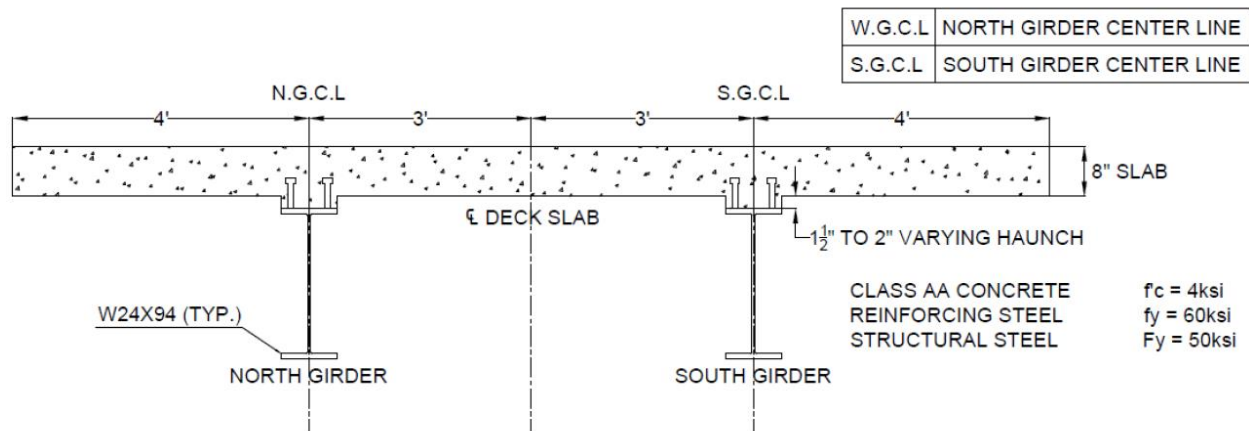
Figure 4.8: Cross section of composite bridge section from the full-sized prototype

Figure 4.8 displays the cross sections dimensions and properties of the prototype bridge. Composite action and shear transfer were affected by pairs of shear studs 7/8 in. diameter x 5 in. long welded to the top flanges at 6 in. The steel girders were spaced at 6 ft. apart and constructed with steel diaphragms at the ends and mid-span locations. Diaphragms matched those provided in the field and consisted of a C12x20.7-tab connections from the channel web to the webs of the W sections. Diaphragms and connections can be seen in **Error! Reference source not found.**.

4.2.1. Concrete Materials:

The concrete mix design conformed to the Class AA specifications contained in the Construction Specifications of the Oklahoma Department of Transportation (ODOT). ODOT concrete mix design proportions are shown in Table 5.1. Cement conforming to ASTM C150, Type I/II was used for the concrete. Locally available aggregates were used. The coarse aggregate is a crushed limestone from a quarry near Drumright, Oklahoma that conforms to ASTM C33, #57 gradation. The fine aggregate also conforms to ASTM C33 and is known locally as "Guthrie sand" used in commercial concrete.

Table 4.3: Class AA ODOT Mix Proportions

Ingredient	PCY	Volume (ft3)
Cement	541	2.29
Flyash	113	0.68
Coarse Aggregate	1845	10.56
Fine Aggregate	1362	8.3
Water	238	3.81
WRA (lq. Oz.)	22.6	-

Ingredient	PCY	Volume (ft3)
HRWRA (lq. Oz.)	15.8	-
AEA(lq. Oz.)	6.5	-
Air	5%	1.35
Total	**4009**	27
	Yield (PCF)	**148.4**

Source of Coarse Aggregate is Quapaw # 57 from Drumright, Oklahoma with a Maximum Aggregate Size of ¾ in. Source of Fine Aggregate is Guthrie, Natural Sand with a Fineness Modulus of 1.60.

The concrete was batched locally and delivered to the Cooper Lab for placement. The concrete mix targeted 5% air content and was achieved using an air entrainment agent. To ensure workability and ease of placement and finishing, a concrete slump of 7 to 8 in. was specified and achieved using both normal range and high range water reducing agents. The minimum 28-day specified compressive strength ($f'c$) for the ODOT Class AA concrete is 4000psi.

It is noted that the ODOT AA specification for concrete provides a range of proportions for mixture constituents. In our mixture design, 20% of the required cement content was replaced with fly ash. It would be reasonable to expect that ODOT AA concrete mixtures with different mixture proportions and constituents would exhibit different time dependent properties and differing hardened properties.

4.2.2. Bridge Instrumentation:

Altogether 100 electronic gages and sensors were employed to measure and monitor concrete and steel strains, concrete and steel temperatures, overall bridge deflections at several locations, and inclination of the steel girders. Instrumentation was installed prior to casting the concrete deck. The instrumentation included the following:

- (7) Thermocouples to measure the temperature within the concrete and ambient temperatures near the bridge deck.

- (8) Vibrating wire strain gauges (VWSG) embedded within the concrete deck prior to casting to measure the concrete strains and concrete temperatures within the hardening deck.

- (9) Electrical resistance bonded foil strain gages (ERSGs) to measured strains in the steel girders.

- (10) ERSGs to measure strains on the surfaces of hardened concrete.

- (11) Linear Variable Differential Transducers (LVDTs) to measured deflections of the bridge girders at various locations; and,

- (12) Inclinometers to measure angle of inclination at the ends of girders.

All the sensors were wired into a datalogger through various multiplexers required for each type of sensor. The sensors were programmed to record data continuously through the period of deck casting. The datalogger was programmed to collect data at 5-minute time intervals for the first 28 days after bridge deck cast. Figure 4.9 shows the sensors locations along the mid-span cross section of the prototype bridge. LVDT sensors were installed at various strategic locations to measure the deflections in the steel girders and bridge overhang. LVDTs' 2 & 3 installed along the girder Center Lines, recorded the deflections of the North and South Girders respectively. LVDTs'1 and 4 recorded the deflections at the edge overhang portions of the deck slab.
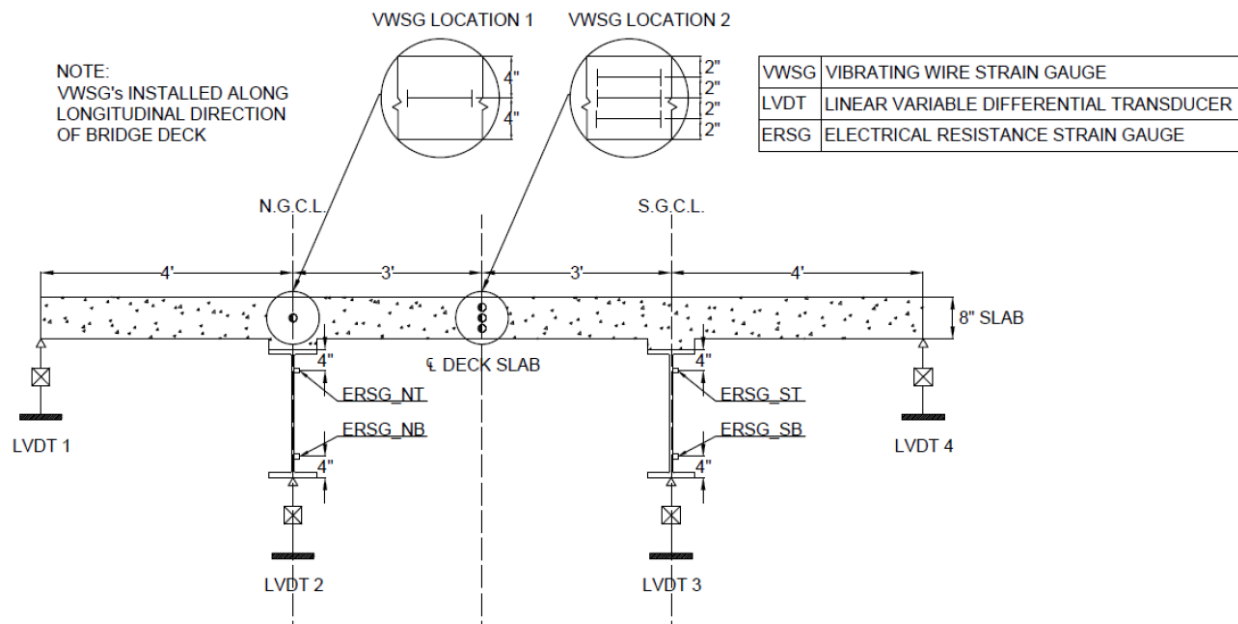
Figure 4.9: Prototype Bridge Cross Section at Mid-span (View Looking East) showing location of sensors.

Figure 4.10 shows a photograph of the LVDT 3 installed at mid-span on the underside of the South steel girder and LVDT 4 at mid-span at the south edge of the slab overhang. Geokon 4200 vibrating wire sensors were embedded within the concrete to capture the strains within the concrete deck. As shown in Figure 4.11a, a single vibrating wire sensor was installed at the mid-height of the concrete slab located along the North Girder's centerline. Figure 4.11b shows three vibrating wire strain gages that were installed vertically at 2 in. c/c spacing along the centerline of the deck, to capture the strain gradient throughout the depth of the concrete slab. The vibrating wire sensors were placed in the longitudinal direction of the bridge deck and fixed in position by tying two short pieces of rebar to the main reinforcing steel using nylon tie-wraps. Thermocouples were also installed close to the vibrating wire sensor locations to measure the concrete temperatures.

Figure 4.10: Installation of LVDT sensors at the midspan location of South Girder (LVDT 3) and South edge of slab overhang (LVDT 4)

a) VWSG Location 1 Aligned with NGCL   b) VWSG Location 2 at CL of Deck Slab

Figure 4.11: Installation of LVDT sensors at the midspan location of South Girder (LVDT 3) and South edge of slab overhang (LVDT 4)

Electrical resistance bonded foil strain gages were attached to the top and bottom of the webs of the North and South girders to capture the steel girder strains. As shown in Figure 4.12 NT & NB, and ST & SB represents the Electrical Resistance Strain Gages (ERSG) bonded to the top and bottom webs of the North and South girders respectively. The gages were about 16 in. apart and bonded at 4.0 in from the top and bottom of the flanges of the steel girder.
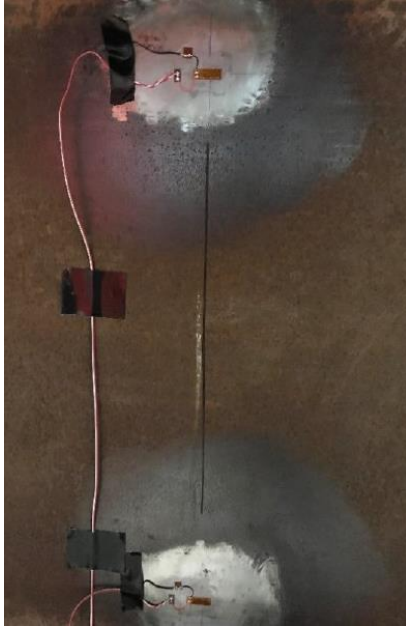
Figure 4.12: Location of Bonded Foil Electrical resistance strain gages on steel girder (NT/ST and NB/SB)

The structural health-monitoring program implemented in this research combines sensors from diverse technologies into a seamless system using a single database and user interface system. The instrumentation system was programmed to monitor both early age and long-term performance of the prototype bridge. The structural health monitoring of a field bridge was implemented through the experience from the laboratory prototype bridge.

4.2.3. Slab Casting

The concrete deck was cast on July 13, 2017, beginning at 10:55 a.m. The concrete placement was completed in 2.0 hrs. and broom finish was completed at 4.0 hrs. Concrete placement started at the West support and proceeded to the east. Concrete was placed via a ¾ CY bucket supported by the overhead crane at the Cooper Lab. There was no delay in using two trucks for the pour. Figure 4.13 shows the concrete deck immediately after casting and prior to finishing. A broom finish was applied to the deck.

Figure 4.13: Bridge deck after casting and finishing concrete. A broom finish was applied.

Concrete sampling was performed from materials obtained from both trucks. Sampling occurred at times near the beginning of each truck and near the middle of each truck. Table 5.2 reports the fresh concrete properties measured from the two trucks during the time of pour. A total of 118, 4 in.x8 in. concrete cylinder specimens were prepared in accordance to ASTM C192. The cylinder specimens were demolded after 24 hrs. and cured in accordance with ASTM C 157.

Hardened concrete properties were measured from cylinders specimens prepared from concrete materials taken from the two trucks. A total of six 12 in. x 4 in. x 4 in. shrinkage prisms were also prepared during the deck cast using the same concrete that was used in the prototype bridge deck. The prisms were cured in accordance with ASTM C 157. Target points for the Detachable Mechanical Strain Gage (DEMEC) were attached on to the shrinkage prisms after 24 hrs. of curing to measure the unrestrained shrinkage strains.

The ODOT specifies a curing regimen that requires wet curing for 10 days. Figure 4.14 shows that wet burlap was placed directly on the surface of the concrete. The burlap was subsequently covered with plastic sheeting. Curing was applied at 4.0 hrs. after the beginning of casting. Prior to the application of burlap, the concrete deck surfaces were inspected. No early age cracking was reported. The deck was wet cured for 14 days after casting, and during that time the deck was covered by wet burlap on the top and by formwork on the bottom. Formwork on the underneath of the deck and on the sides of the deck remained in place during curing. Removal of formwork and bracing began after 11 days, but the wet burlap and plastic sheeting remained in place for 14 days. After removal curing materials, the concrete deck was inspected for cracking. No cracks were found.

Figure 4.14: Wet burlap and 2 mil plastic was applied for 14 days

This research focuses on determining the impact of thermal loading on durability and serviceability of steel girder bridges made composite with concrete slabs. Concrete bridge decks are subject to repeated temperature changes that cause temperature gradients through the depth of the slab and through the depth of the cross section. These temperature gradients produce internal thermal strains and stresses that directly result in bridge deformations. Generally, restraint from the composite girders cause compression in the slabs during heating and tension in the slabs during cooling. This phenomenon can adversely affect the ride quality, cause deck cracking and excessive deflections, decrease durability, and reduce long-term performance of bridges.

Bridges are subjected to repeated cycles of heating and cooling from solar radiation from temperature differentials from the surrounding air, variations in humidity and wind. For concrete-steel composite bridges, this exposure produces thermal movements and stresses in bridges due to external restraints, temperature gradients and dissimilar material properties. The volumetric changes in concrete due to these temperature gradients cause upward and downward bridge deflections, differential strains, and internal stresses within the concrete deck. These temperature induced stresses depend on the end conditions of the bridge structure and the temperature distribution.

The current *AASHTO LRFD Bridge Design Specifications* (American Association of State and Transportation 2014) provide temperature ranges to account for the overall expansion and contraction due to the presence of thermal changes through the depth of the structure.

A large array of sensors and instruments were installed on the prototype bridge to measure strains, deflections and temperatures in both concrete and steel. Overall bridge deflections were measured with Linear Voltage Displacement Transducers (LVDT's) at midspan and at other points along the length of the steel girders. Concrete temperature gradients throughout the depth of the slab were monitored using thermocouples. Concrete strains were measured with vibrating wire strain gages (VWSG's) embedded in the concrete deck. Steel Strains were measured using Electrical Resistance Bonded Foil (ERBF) gages installed on the webs of the steel girders. Measurements and monitoring are continued through 56 days of heat loading and testing.

4.3. Results and Discussions:

4.3.1. Fresh and Hardened Material Properties:

Table 4.4: Fresh Concrete properties

Measured Properties	Truck 1	Truck 2
Slump (inches)	9.5	8.25
Unit Weight (lb/ft3)	144.2	141.8
Concrete Temperature (º F)	91.5	91.3
Air Content (%)	8	9

Table 4.5: Hardened Concrete properties

Age (Days)	C39 – Truck 1 (psi)	C39 – Truck 2 (psi)	C 469 – Truck 1 (ksi)	C 469 – Truck 2 (ksi)	C496 – Truck 1 (psi)	C496 – Truck 2 (psi)
1	1485	2095	2404	2620	217	339
3	3440	3870	3059	3355	411	447
7	4195	4465	3378	3774	512	588
28	5245	5605	3843	4027	541	602

Notes:

- Compressive strength (psi) measured in accordance with ASTM C39
- Elastic Modulus (ksi) measured in accordance with ASTM C469
- Splitting cylinder tensile strength measured in accordance with ASTM C496

4.3.2. Thermal Effects at Early Age from Concrete Hydration

In its initial stages, the chemistry of Portland cement generally provides a "dormant" period that allows for transportation and placement of the concrete in its fresh state. As the cement hydration continues, initial set of concrete is generally characterized by the onset of rapidly increasing temperatures. After initial set, increasing temperatures cause volume expansion in the concrete at early ages. However, thermal expansion of the concrete is restrained by the composite steel girders, and thus the increasing hydration temperature induces internal compression stresses within the restrained concrete. Similarly, the newly composite steel-concrete bridge deflects upward as concrete temperatures increase with cement hydration. Our experimental program measured concrete temperatures, concrete strains and overall bridge deformations.

4.3.3. Measured Temperature and Strains at Early Ages:
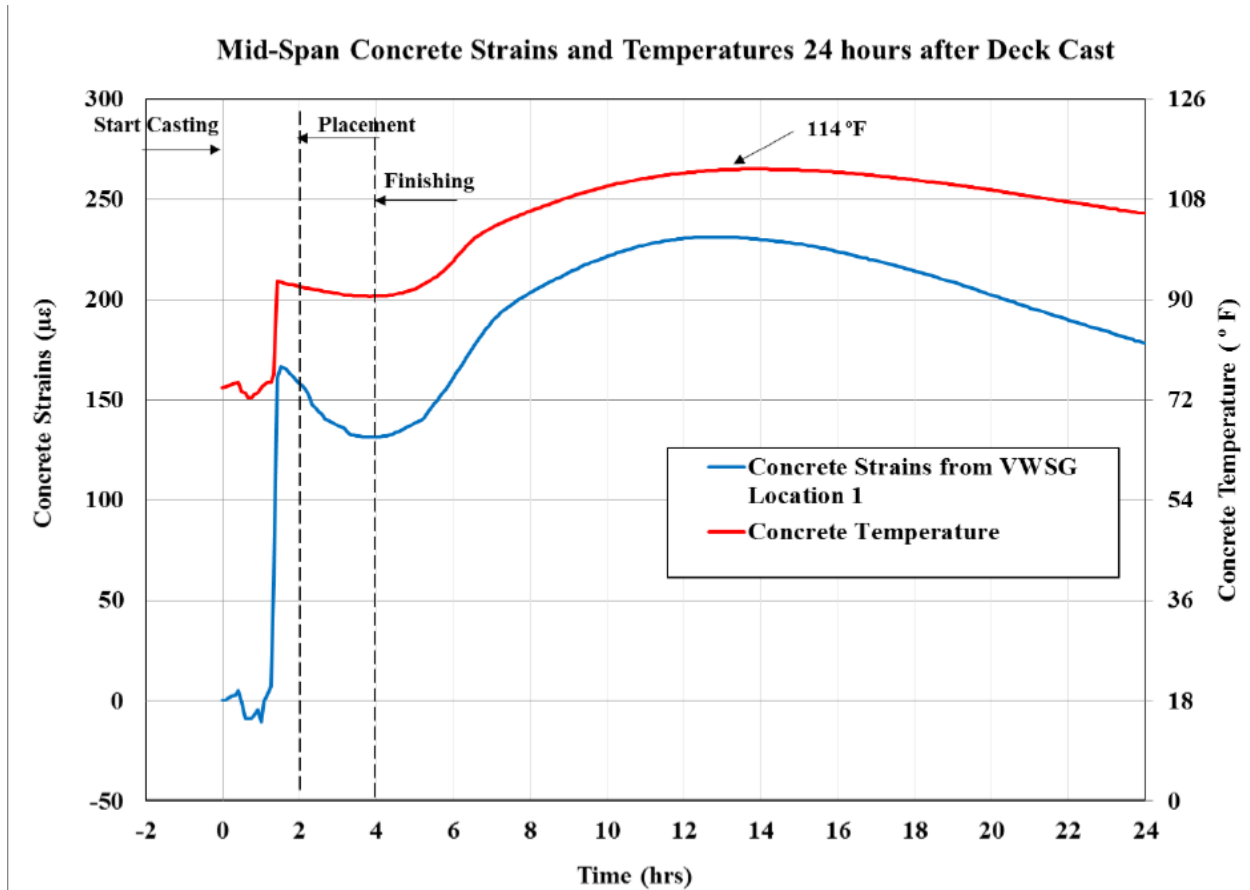
Figure 4.15: Concrete Temperatures and strains measured at mid-height of deck slab recorded until 24 hours after deck cast

Figure 4.15 shows the concrete temperature and concrete strains measured over time beginning at two hours before slab cast and for the continuing through the first 24 hrs. from slab casting. The concrete temperature and strains were measured by the vibrating wire sensors embedded in the concrete at the mid-height of the slab at the mid-span location along the North Girder (VWSG Location 1). The figure shows that the concrete temperatures elevated to about 114⁰ F reaching peak temperatures at approximately 14 hrs. The measured thermal strains within the concrete correspond well with the concrete temperatures. The measured concrete strains increased with temperature rise and decreased with the fall in concrete temperatures.

Figure 4.16 captures the full heating and cooling cycle during concrete hydration along with measured concrete temperatures and strains for the first 96 hrs. after slab cast. The figure highlights that the measured thermal strains within concrete increase with the increase in temperatures and decrease with fall in concrete temperatures. During the process of cement hydration, initial setting of concrete is often defined as occurring with the peak temperature.

After initial set, the concrete gains stiffness during the cooling cycle. At the end of the heating cycle, concrete will begin to cool and shrink which is indicated by the decrease in thermal strains and increase in compressive concrete shrinkage strains. This shrinkage can be caused by either or both thermal strains and shrinkage strains. As the steel girders restrain the shrinkage of concrete, tensile stresses within the concrete will begin to develop immediately at the end of the temperature rise. However, no cracking on the surface of concrete deck was reported during this time. Hence it is seeming evident that the tensile stresses caused by the restrained shrinkage are not sufficient to cause bridge deck cracking on the prototype full-sized bridge, at least using these constituent materials subject to these atmospheric conditions.
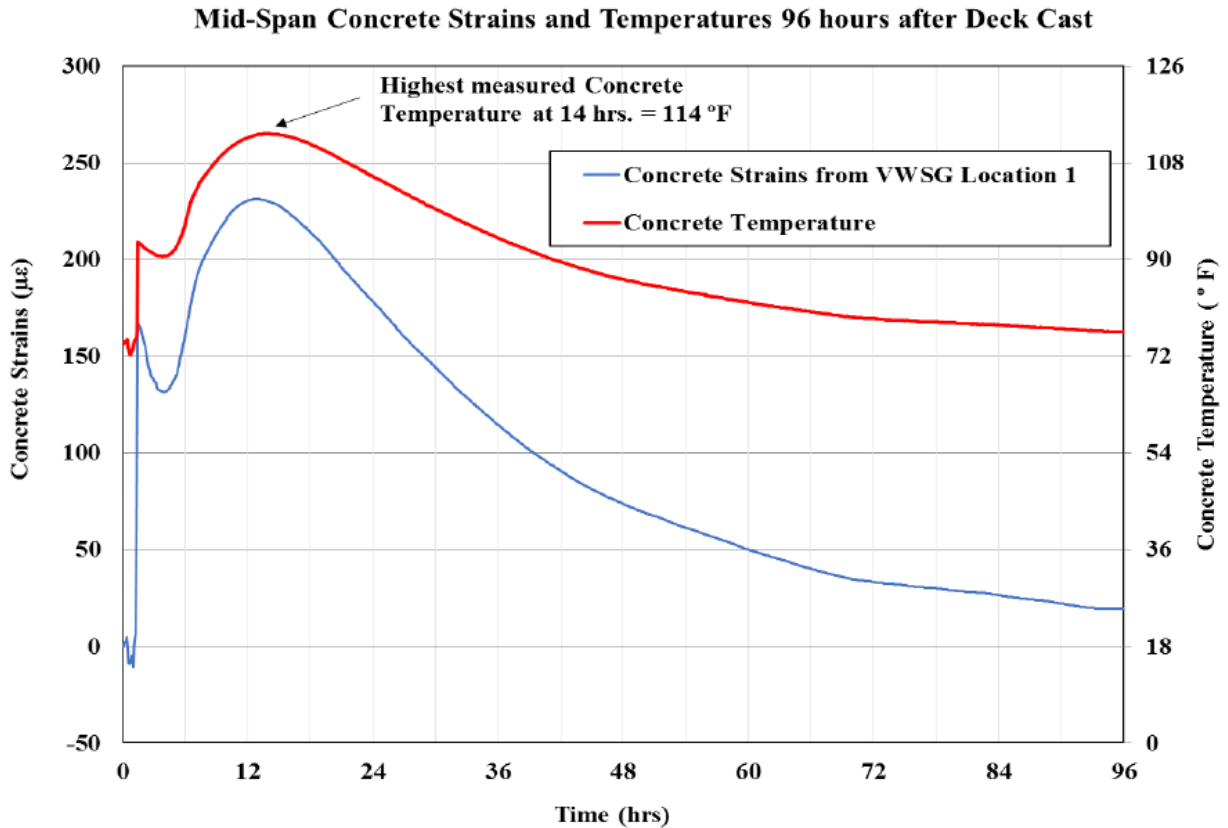

Figure 4.16: Concrete Temperatures and strains measured at mid-height of deck slab recorded for 96 hours after deck cast.

5. Material Testing

5.1. Introduction:

Even though creep and drying shrinkage have been studied for a long period of time, there are still many aspects of these factors that not fully understood. Furthermore, tensile creep studies are especially limited. For instance, there is an ASTM standard for compressive creep testing, but there is no ASTM counterpart for tensile testing exists.

Also, while the compressive modulus of elasticity has been studied extensively, the tensile modulus of elasticity is completely ignored. This is because engineers tend to ignore the tensile strength of the concrete.
Specific for this research, we initiated the work to perform tensile creep tests on concrete through its early ages to determine what effects creep can have on lessening the tensile stresses that new concrete decks will experience. Essentially, tensile strains measured during curing of the new bridge decks were in the range where cracking MAY be expected; however, no cracking was discovered. Naturally, any creep effects in tension work to effectively reduce the stresses in the concrete (for the same strains) and at the same time reduce the tensile stresses that may cause cracking.

5.2. Methodology:

We have performed significant laboratory testing in Phases 1 and 2. In Phase 3, we reestablished the aggregate properties for the coarse and fine aggregates and developed and tested the proposed the different mix design proportions for the creep in compression and tension testing.

Table 5.1 lists the types of mixes and mix ingredients. The control mix with fly ash represents Class AA ODOT mix followed by the mix with the same mix without fly ash. In addition to these two other mixes, one with a lower w/cm of 0.4 and another using optimized gradation that includes the addition of 3/8" aggregate to the mix will also be cast and tested. Table 5.2 shows the mix design proportions that were established from the ODOT AA concrete mix. The fresh properties for the tension and compression batches for each mix are tabulated in Table 5.3.

Table 5.1 Concrete Mixture Constituents

Control w/Fly ash	No Fly ash	Low w/cm	Optimized
Cement	Cement	Cement	Cement
Fine aggregate	Fine aggregate	Fine aggregate	Fine aggregate
Coarse Aggregate	Coarse Aggregate	Coarse Aggregate	Coarse Aggregate+ 3/8 aggregate
Fly Ash	-	Fly Ash	Fly Ash
Water	Water	Water	Water

Control w/Fly ash	No Fly ash	Low w/cm	Optimized
AEA	AEA	AEA	AEA
WR	WR	WR	WR
HRWR	HRWR	HRWR	HRWR
w/cm = 0.44	w/cm = 0.44	w/cm = 0.40	w/cm = 0.44

Table 5.2 Mixture Proportions (PCY)

	Mix Proportions (lb/yd³)					Admixtures (oz)		
Mix Type	Cement	Fly Ash	Coarse	Fine	Water(gal)	AEA	WR	HRWR
Control	450	114	1854	1335	29.4	2.5 oz	22.6 oz	-
No Fly Ash	564	-	1854	1348	29.4			
Low w/cm	450	114	1854	1383.60	27			

Table 5.3 Fresh Concrete Properties

| Mix ID	FA (T)	NOFA (T)	LOW W/CM (T)	OPT (T)	FA (C)	NOFA (C)	LOW W/CM (C)	OPT (C)
Slump (in.)	3	2.5	0.25	4	2.75	0.75	0.63	3.5
Unit Weight (lb/ft³)	148.9	147.4	149.1	142.8	147.8	153.1	150.5	142.8
Concrete Temperature (°F)	73.6	75.8	77.8	76.9	80.6	79.5	77.8	76.9
Ambient Temperature (°F)	73.6	73.5	74	74	73.9	73.4	74	72
Air Content (%)	6.2	7.0	5.7	9.0	6.5	3.5	5.0	8.6

Notes:

- (T) – Tension Batch Specimens
- (C) – Compression Batch Specimens

5.2.1. Tension Specimens (Dogbones):

For this research we have used specimens similar in shape and geometry as those employed by Nelson (2013). Each specimen was cast inside a wooden mold with a VWSG oriented longitudinally down its centerline. This specimen design was chosen in order to limit the chance

of cracks developing in the specimen and allow adequate space for the VWSG to be cast inside the specimen. In contrast to Nelson's design, the dogbones in this research employed precast threaded inserts to apply the load to the specimen, rather than concrete caps. These provided better load transfer directly along the specimen's centerline. No rebar was used in any of the dogbones. The typical dogbone dimensions are shown in Figure 5.1. The physical dogbone molds with the VWSGs installed prior to casting are shown in Figure 5.2
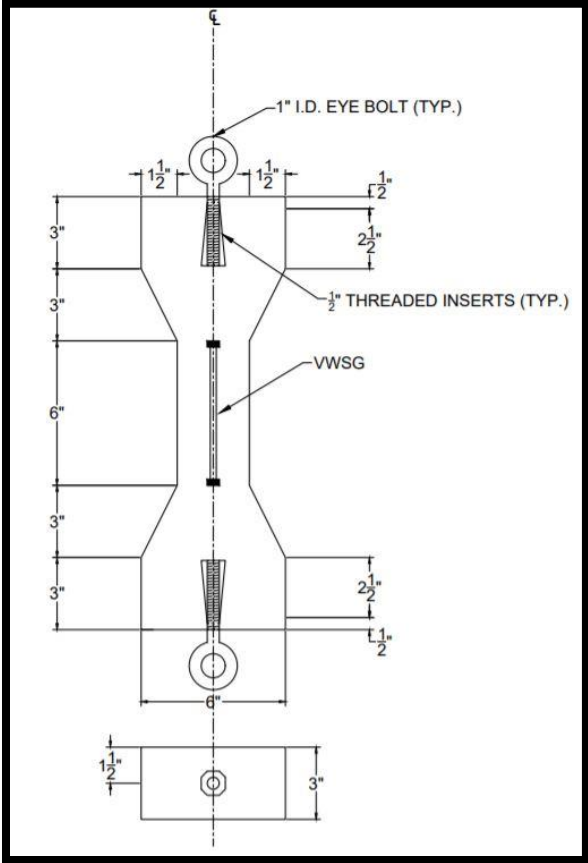
Figure 5.1 Dogbone Design Schematic and Dimensions

Figure 5.2 Dogbone Forms Prior to Casting with Vibrating Wire Gages Installed

The dogbones were cast in two lifts. The first lift was filled to approximately halfway up the cross-sectional depth of the specimen, and the second to the top. The specimens were vibrated on a vibrating table immediately following each lift and were hand-finished with a trowel. Each dogbone was to 50% of its estimated tensile breaking stress according to the following formula:

$$\sigma_t = (0.50)(4\sqrt{f_c})$$

Where f_c is the concrete compressive strength measured by ASTM C39 at the age of loading and σ_t is the target tensile stress, both in units of psi.

All concrete cylinder specimens were cast in 4 in. x 8 in. plastic cylindrical molds. Compressive breaking strength, splitting tensile strength, and compressive modulus of elasticity tests were conducted in accordance with ASTM C39, C496, and C469, respectively. These tests were conducted at various ages.

The C469 elastic modulus test was conducted using a computer to regulate the applied load and automatically record the strain readings from the LVDT attached to the cylinder. Each cylinder was loaded four times to 40% of the average breaking strength for that day (obtained by breaking companion cylinders from the same mix). The data from the first round of loading was disregarded and the modulus of elasticity was determined by averaging the results of the subsequent three loadings.

All C39 and C469 tests were conducted with neoprene padding. No sulfur capping was employed for any of the cylindrical specimens in this research.

In addition to the shrinkage beams, each mix also had shrinkage cylinders with VWSGs cast inside of them as well. These VWSGs were oriented longitudinally along the centerline of the cylinders. The shrinkage cylinders were stored in the same room as the tensile and compressive creep specimens

Each of the concrete testing samples were placed in a controlled environment to ensure standard curing and temperature conditions. Three different curing conditions were employed: a) a fog room where temperatures were maintained at 73˚F and concrete surfaces remained damp, b) covered in wet burlap (not the fogroom) with temperature maintained at 73˚F, and c) the "dry curing" room with temperature at 73˚F and RH = 50%.

Figure 5.3 shows the Dogbone Specimens loaded in the Tensile Creep Frame. The frame allowed adjustment of tension forces on each individual Dogbone specimen. Total tension force applied was the product of the target stress times the measured cross-sectional area.

Figure 5.3: Dogbone Specimens Loaded in the Tensile Creep Frame

5.2.1. Compression Specimens:

Frames for testing the creep of concrete in compression were designed based on recommendations from ASTM C512. Each frame consisted of 5 steel plates attached to 3/4" diameter threaded steel rods. An Enerpac RCH603 hydraulic cylinder jack was used to apply the load to the concrete cylinders and hydraulic accumulators were employed to help maintain constant hydraulic pressure in the system. Each frame was loaded with three cylinders from a specific concrete mixture. These cylinders were lapped to make their tops and bottoms planar, then they were subsequently fixed together using quick-setting epoxy. This epoxy helped keep the columns rigid in order to prevent buckling in the column. After the epoxy had achieved a strong enough hold (usually after about 10 -20 minutes) the cylinders were placed in the frame and loaded. Several creep frames loaded with cylinder columns are shown in Figure 5.4.

Figure 5.4 Compression Creep Frames Loaded with Concrete Cylinder Specimens

Due to the varying strengths of the mixes and the hydraulic setup the mixes were loaded to different proportions of their breaking strengths. This was necessary to avoid over-stressing weaker mixes that were paired with stronger mixes on the same accumulator (and thus had to have equal pressure). The concrete cylinders, identified by the mixture designs, and their accompanying stresses are summarized in Table 5.4.

Table 5.4 Compression Stresses and Loading Summary for Creep Specimens in Compression

Mix	Applied Stress (psi)	Breaking Stress (psi)	Applied Stress/Breaking Stress
FA	800	1268	63.1%
NOFA	800	2417	33.1%
LOW W/CM	250	1008	24.8%
OPT	250	685	36.5%

5.3. Results and discussion:

The values for the compressive breaking strengths of each mixture's tensile and compressive batches are tabulated in the Table 5.5. The averages between the tensile and compressive batches are also Charted in Figure 5.5. 90-day breaks were only conducted on the

compressive batches. It is noted that the OPT mixtures were lower in strength than the companion mixtures. We do not have explanation for this. Results from Splitting Cylinder Tensile Strength tests are reported in Table 5.6. Figure 5.6 charts the Elastic Modulus (ksi) of concrete vs. Time.

Table 5.5 Concrete Compressive Strengths (psi) for Tension and Compression Specimens

Age (days)	FA (T)	NOFA (T)	LOW W/CM (T)	OPT (T)	FA (C)	NOFA (C)	LOW W/CM (C)	OPT (C)
1	870	1419	1008	685	1268	2417	1432	508
3	N/A*	N/A*	3664	2279	3247	4517	4316	2156
7	4395	4498	4913	3288	4061	5784	5426	3425
28	3613	3812	6175	4310	5360	6873	7074	4294
56	6442	5812	7038	4628	5981	7738	7836	4769
90	N/A**	N/A**	N/A**	N/A**	6299	8774	8178	5367

Notes:

- N/A** - Results not available.
- (T) – Tension Batch Specimens
- (C) – Compression Batch Specimens
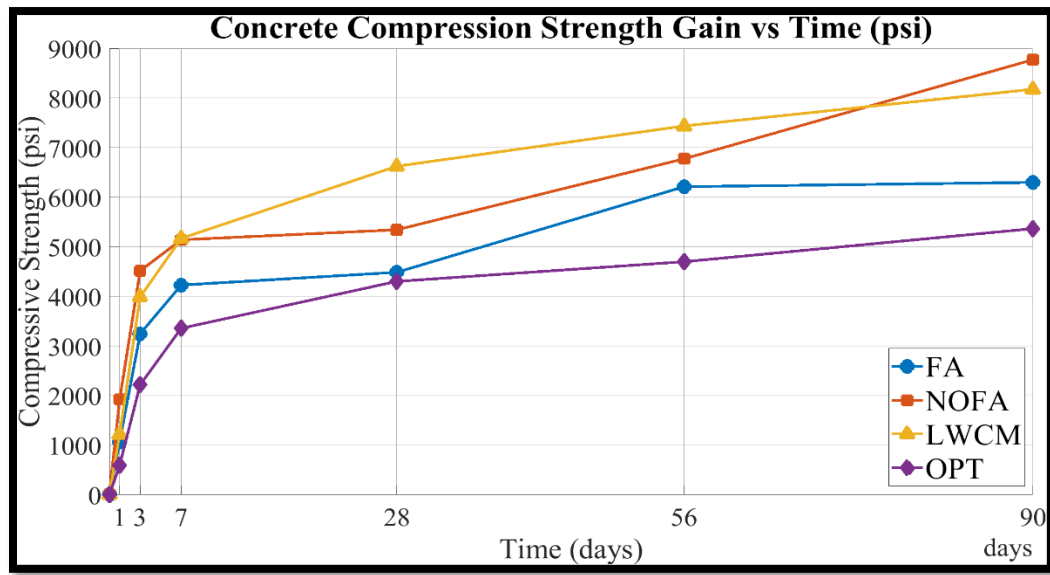
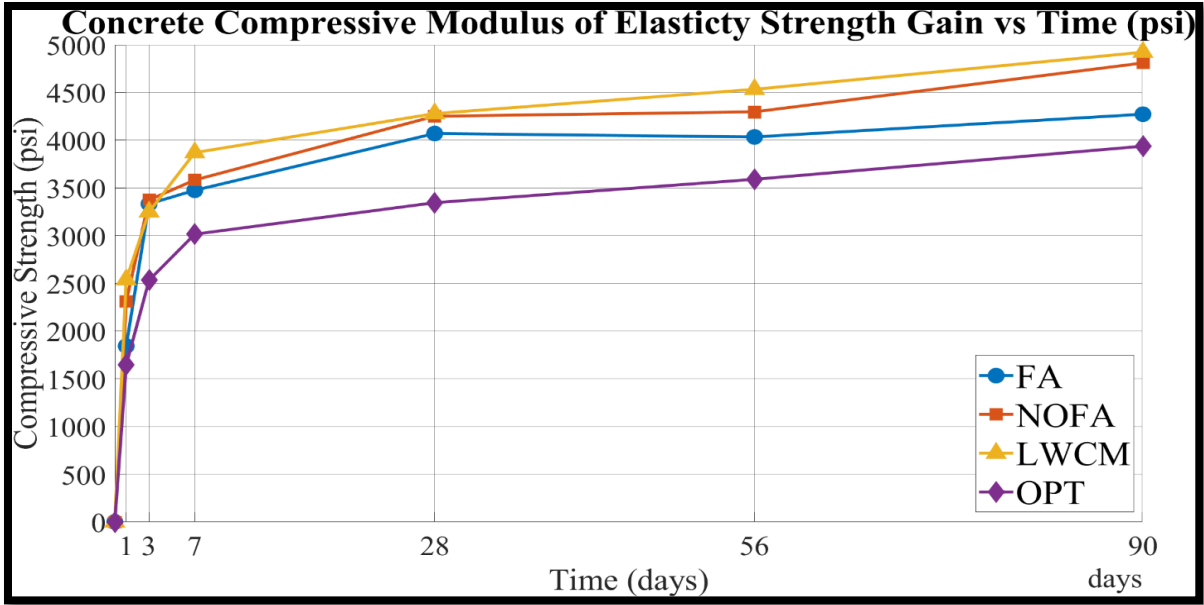**Figure 5.5: Concrete compressive strength gain over time (averaged between tensile and compressive batches)**

45

Figure 5.6 Concrete Elastic Modulus (ksi) vs. Time (days)

**Table 5.6 Splitting Tensile Strengths (psi). ASTM C496**

Age (days)	FA (T)	NOFA (T)	LOW W/CM (T)	OPT (T)	FA (C)	NOFA (C)	LOW W/CM (C)	OPT (C)
1	175	248	164	104	195	382	198	116
3	448	481	249	150	159	340	N/A*	N/A*
7	397	451	535	396	542	605	567	339
28	629	492	716	500	605	799	503	422
56	649	514	703	593	672	689	684	595

Notes:

- N/A* - Results not available.
- (T) – Tension Batch Specimens
- (C) – Compression Batch Specimens

Figure 5.7 charts strains vs. time measured for the dogbone specimens. Note that all of dogbone specimens show shortening of the dogbone specimens. For example, the No-Fly Ash (NOFA) specimens exhibit, on average, approximately 300 microstrains of shortening over 56 days. Figure 5.7 also charts the shrinkage strains of the companion shrinkage cylinders, and the magnitude of these shortening strains are larger than that of the dog bone specimens. For example, the No-Fly Ash shrinkage specimen (NOFA) indicates approximately 440 microstrains of shortening. So both the dogbone specimens, which are loaded in tension, and the shrinkage specimens – where are not loaded – exhibit shortening strains. Looking at all the data, for each set of companion specimens, the shrinkage strains are more negative than the tensile dogbone strains. So from these data, the effects of the tensile stresses applied to the dog bone specimens are represented by the difference in strain between the dog bone and the shrinkage cylinder.

The tension dogbones were loaded at 1-day of age and were monitored over a duration of 56 days. Both the tension dogbones and the companion shrinkage cylinders were maintained in the dry-curing room at 50% RH. Note that each specimen's strain values were zeroed at the time of casting. The temporary gaps in strain data readings seen in the figure were due to power losses in the data logger. By subtracting the shrinkage strain values from the raw total strain values, the net strain due to loading for each specimen can be determined.
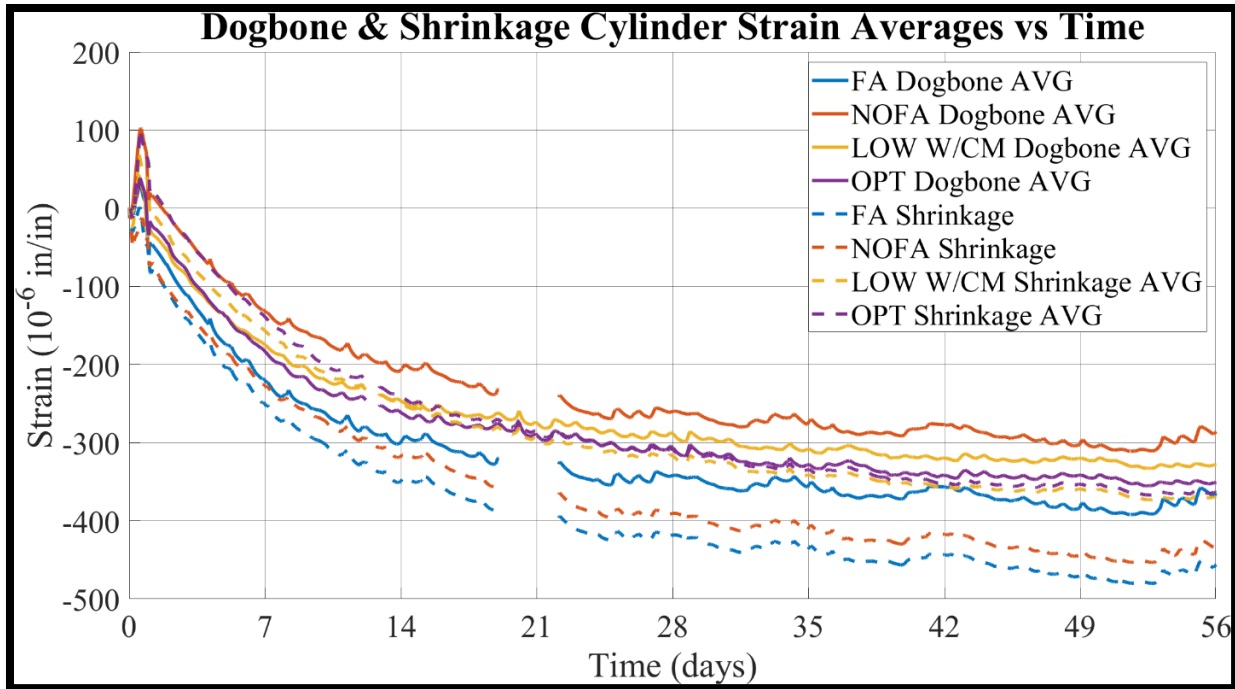
Figure 5.7 Concrete Strains vs. Time. Tension Dogbones and Companion Shrinkage Cylinders.

Figure 5.8 charts strains vs. time measured for the compression creep specimens. The figure also shows the shortening strains measured on the companion shrinkage cylinders. Note that the compressive creep specimens exhibit larger compression strains, or shortening strains, than the shrinkage cylinders. For example, the No-Fly Ash (NOFA) compression creep specimens exhibit, on average, approximately 1200 microstrains of shortening over 90 days. Noting that the companion shrinkage cylinder exhibits approximately 500 microstrains of shortening at 90 days, one can conclude that the combination of elastic compressive strain plus compressive creep strains is represented by the difference, or about 700 microstrains.

Compression was applied at 1 day of age, and the chart shows the short-term elastic shortening strains. For the NOFA concrete, this appears to be about 350 microstrains. From there, the additional shortening to 1200 microstrains can be attributed to a combination of creep and shrinkage.

In order to verify that the strains measured in the concrete shrinkage cylinders are reasonable accurate, strain readings from the shrinkage beams were also monitored throughout the first month after casting. The DEMEC strain readings from these beams are shown in Figure 5.9.
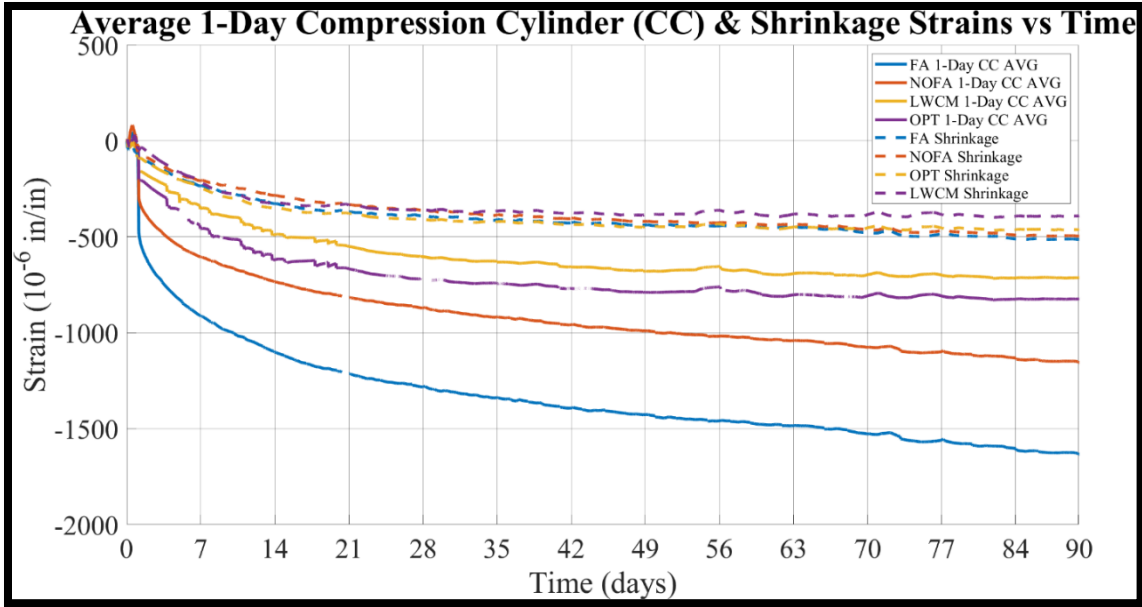
Figure 5.8 Concrete compression creep strains plus strains of the shrinkage cylinder specimens.
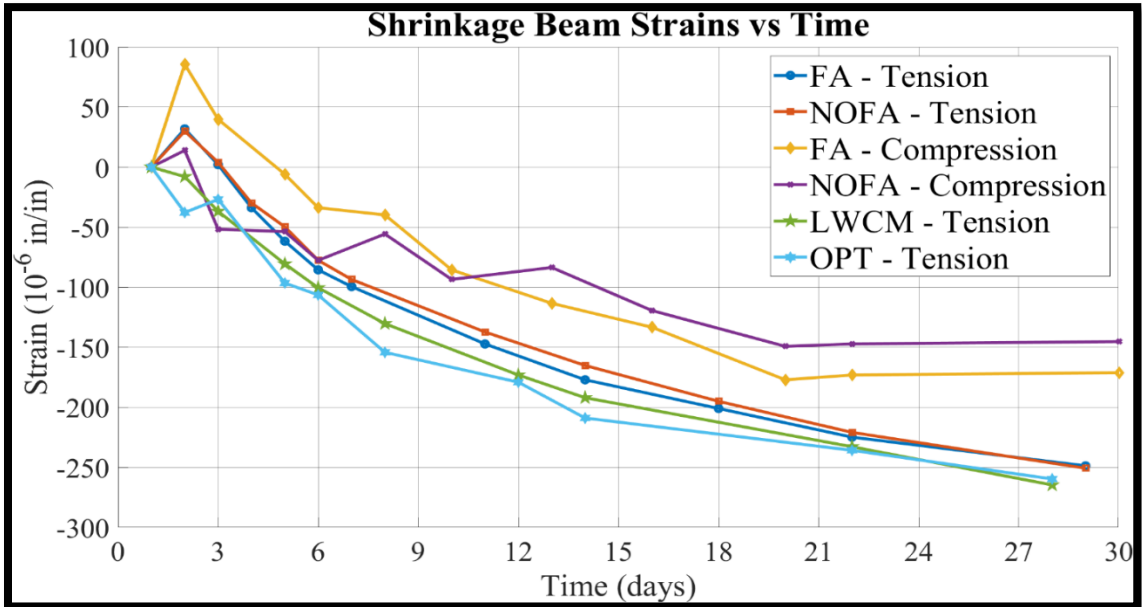
Figure 5.9 Strains measured by DEMEC gages on rectangular shrinkage prisms.

Figure 5.10 charts the difference in strain between the dog bone tension creep specimens vs. the unloaded shrinkage cylinders. From the data, one can see that the tension strains increase over time. The chart shows the differences between strain readings, so there appear to be absolute differences between the various concrete mixtures. Figure 5.11 charts the difference

49

in strain between the compressive creep specimens vs. the shrinkage cylinders. The attempt here is to isolate the effects of creep. Again the chart shows the differences in strain readings.
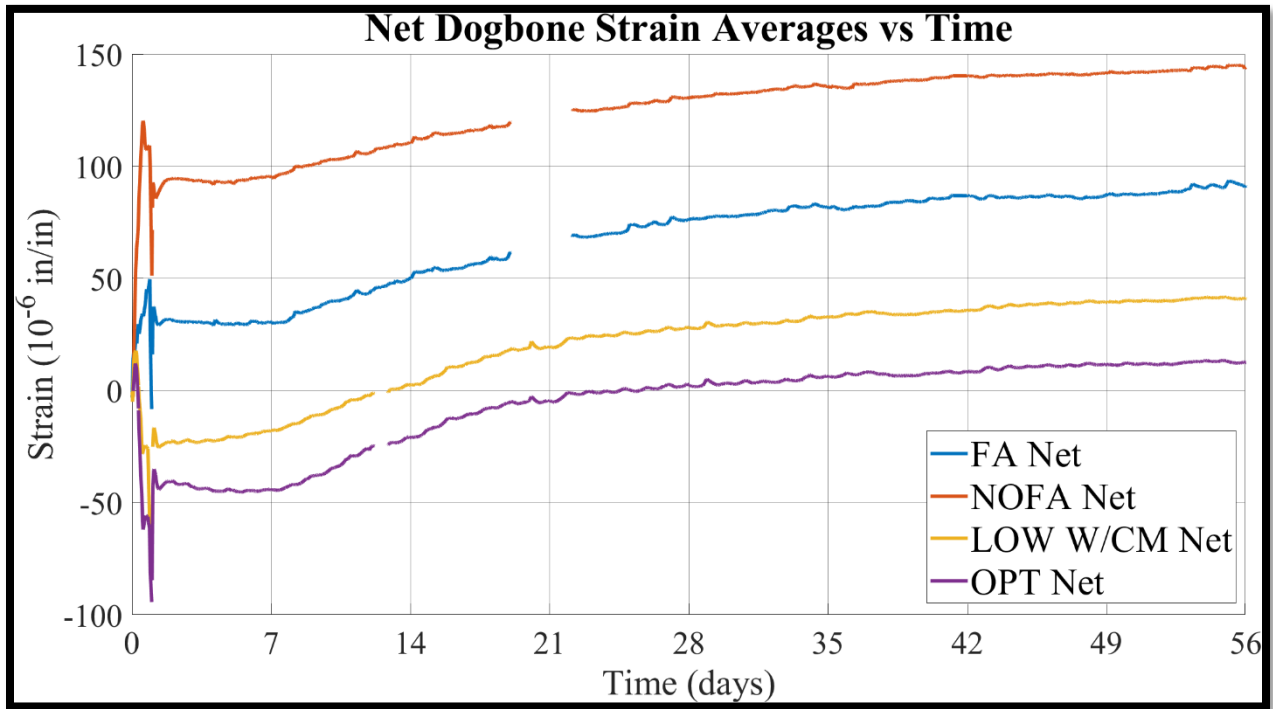

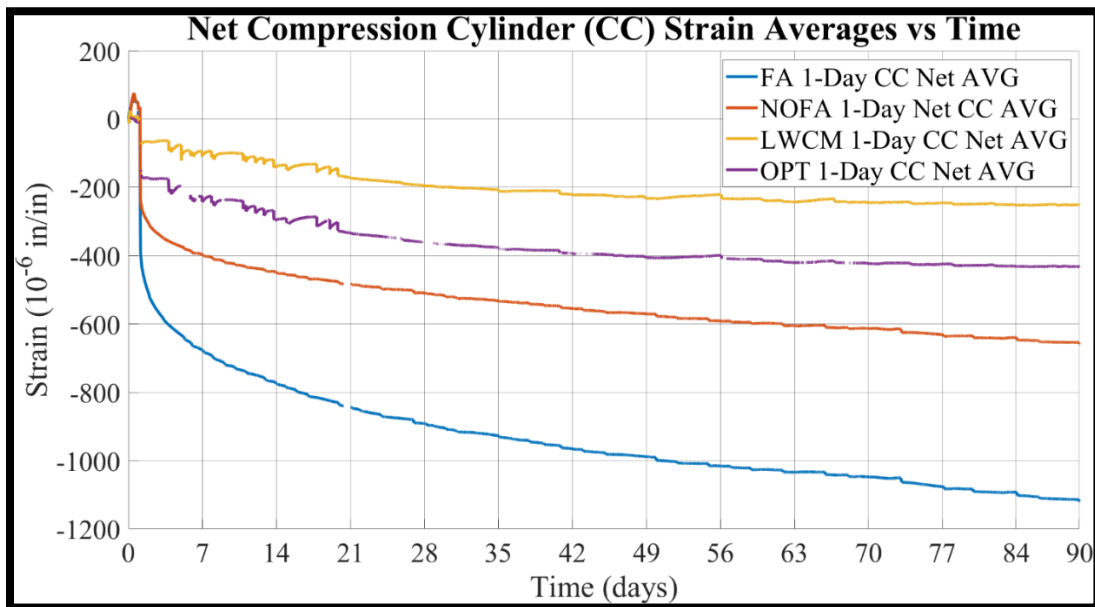**Figure 5.10 Net Tensile strain in Dogbone specimens.**

Figure 5.11 Net Compression Strain vs. Time.

From these data, at least theoretically, the creep coefficient can then be determined for each set of test specimens and plotted over time. These data are shown in Figure 5.12 for the tensile creep test specimens and Figure 5.13 for the compression creep specimens. Creep coefficients were calculated by dividing the initial elastic strain by the net strain for each set of specimens. The computed creep coefficients are found in Table 5.7. One can observe considerably more variation in the tensile creep specimens, most likely caused by the smaller differences in measured shortening strains.
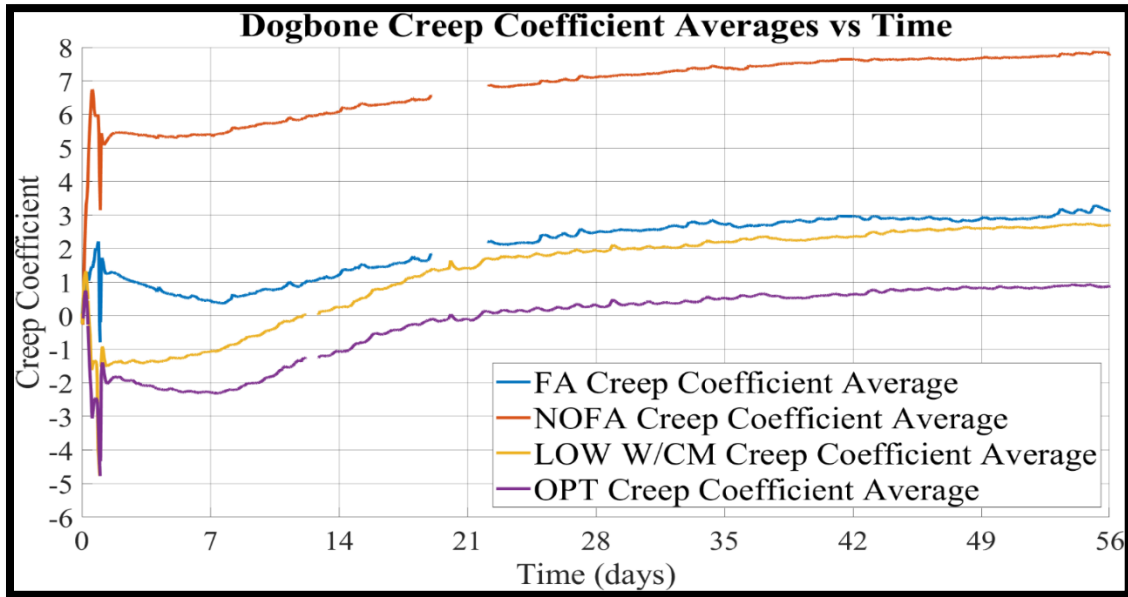

Figure 5.12 Tensile Creep Coefficient over time.
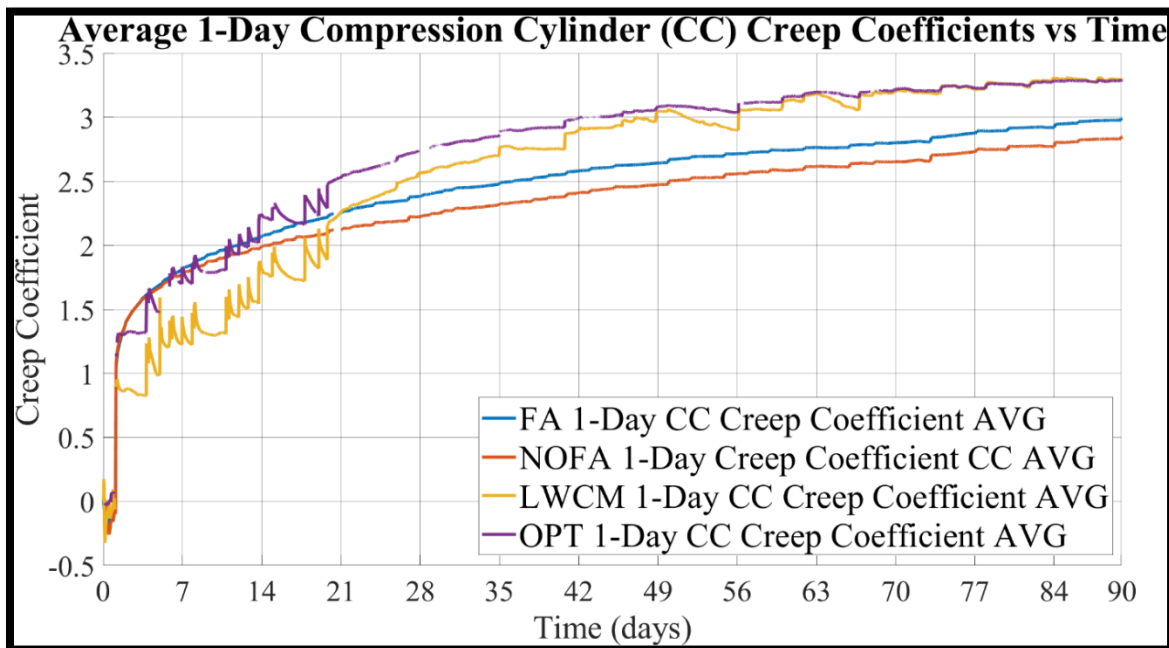
Figure 5.13 Creep Coefficient Average vs. Time (Compression)

Table 5.7 Computed Creep Coefficients.

Mixture	Dogbones (56 Days)	Compression Cylinders (56 Days)	Compression Cylinders (90 Days)
FA	3.14	2.72	2.99
NOFA	7.80	2.56	2.85
LWCM	2.70	2.90	3.30
OPT	0.87	3.04	3.29

5.4. Summary:

From the results above, creep and shrinkage effects have a considerable impact on the strains experienced by the concrete, even at early ages. While creep is often relegated to the realm of long-term concerns, these results show that it still can result in strain values large enough that cannot be ignored.

6. FIELD BRIDGE MONITORING

6.1. Site and Location Description:

The field bridge was located in Blackwell, Oklahoma on State Highway 11 over the Chikaskia River. The bridge featured a 30-degree skew, which had to be considered. The two-lane bridge consisted of a 6-in. concrete deck supported on six 54-in. deep by 3/8-in. thick plate girders. This bridge was scheduled to be rehabilitated with a new bridge deck installed upon the existing bridge girders, so it offered a prime opportunity to study the long-term strains in the concrete and girders while being subjected to traffic loading.

6.2. Instrumentation Description

Three primary sensor types were employed on this project: vibrating wire strain gauges (VWSGs), thermocouples, and inclinometers. Each sensor and its purpose will be discussed in the following sections.

6.2.1. Vibrating Wire Strain Gauges (VWSGs)

Vibrating wire strain gauges were discussed in detail in Section **Error! Reference source not found. Error! Reference source not found.**. The same VWSGs (Geokon 4200s) that were employed in the material testing portion of the project were also used in the SH-11 bridge.

6.2.2. Thermocouples

In order to adequately capture the variation of temperature in the concrete and steel throughout the depth of the cross-section, Type J thermocouples were installed at strategic locations to complement the temperature data obtained via the thermistors on the VWSGs. These thermocouples were both cast into the concrete deck as well as fixed to the steel girders. Figure 6.1 below shows the locations of the thermocouples and VWSGs on each girder.
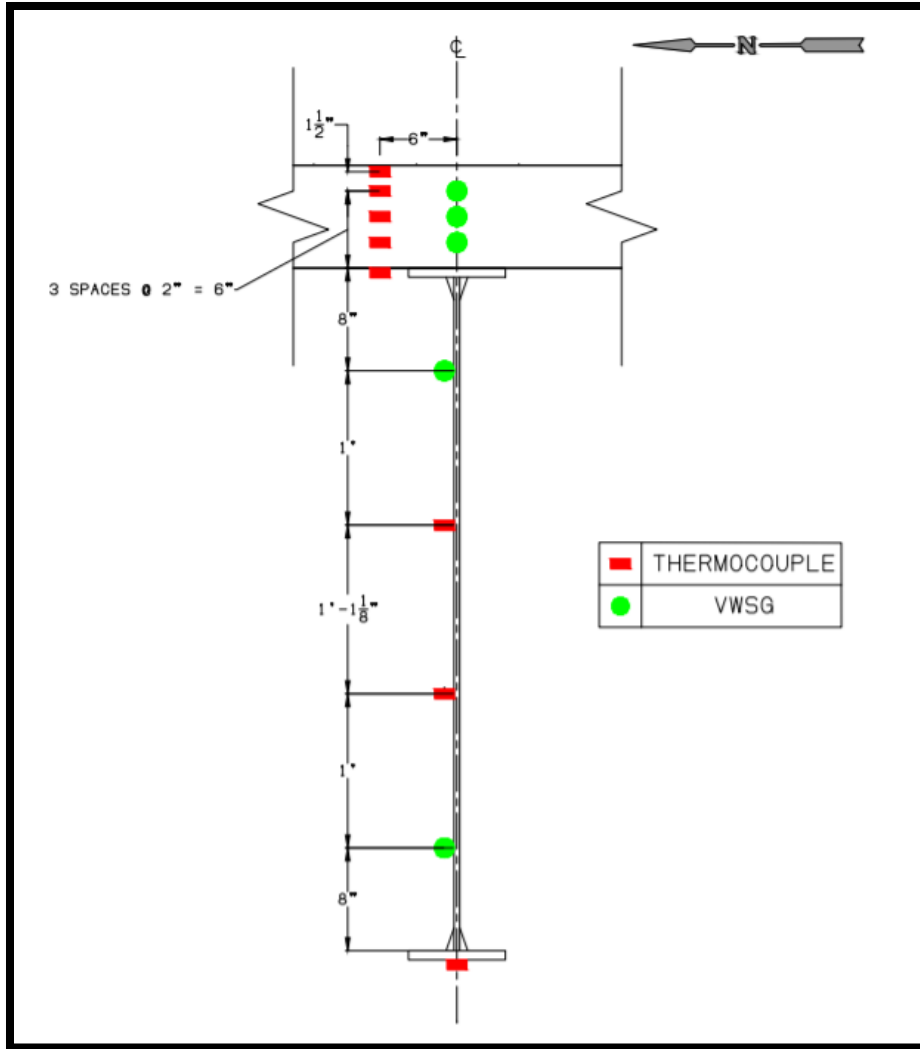
Figure 6.1: VWSG & thermocouple locations on each girder

6.2.3. Inclinometers

The final sensor type employed on this project were inclinometers. Inclinometers are specialized sensors that measure minute changes in angles. By gluing them to the girder webs near the supports, we were able to obtain slope readings that would allow us to approximate deflections in the bridge deck. A diagram describing the locations of each inclinometer are show in Figure 6.2 below.
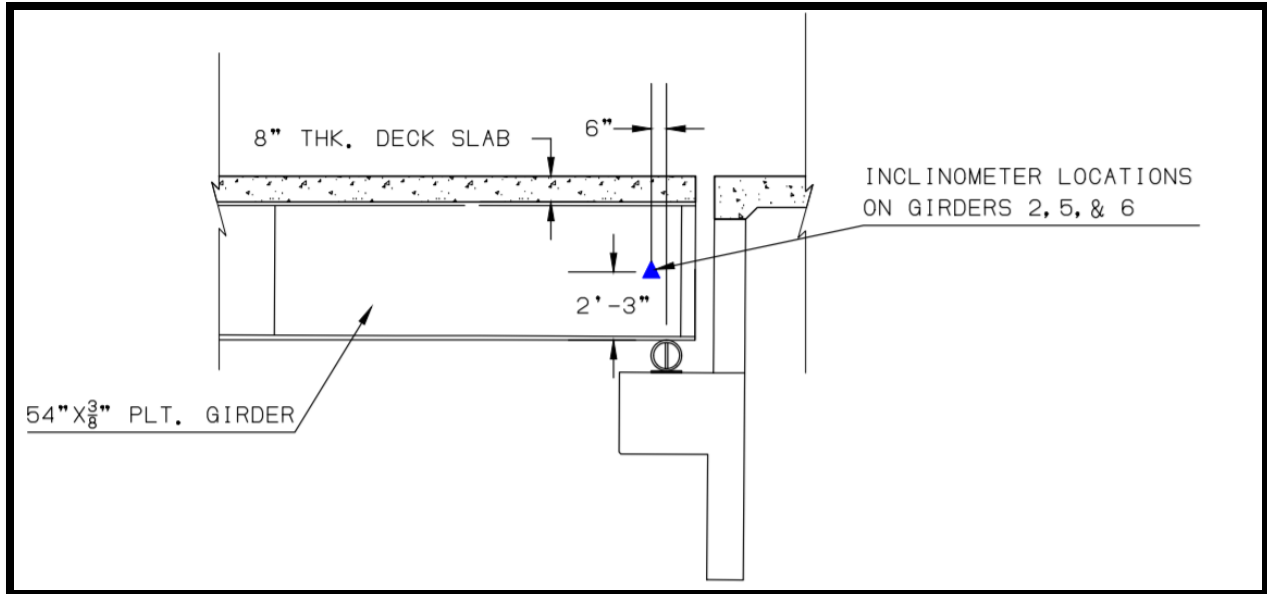
Figure 6.2: Inclinometer sensor location drawing

6.2.4. Campbell Scientific Data Logger

The data logger setup used for the field bridge was very similar to the one used for the prototype bridge, with a few notable exceptions. The data logger was equipped with a wireless modem that allowed the research team to remotely connect to it and view and download the data at any time without needing to be physically present. The data logger was powered using a solar panel. This setup allowed the data logger to remain in the field and collect data without needing to be constantly monitored.

6.2.5. Instrumentation Layout

Three girders were selected to be instrumented, along with the concrete directly above them. These were the two south-most girders (Girders 5 & 6), as well as the second north-most girder (Girder 2). The WVSG and thermocouple sensors were installed at the locations shown in Figure 6.3 below. These girders were instrumented
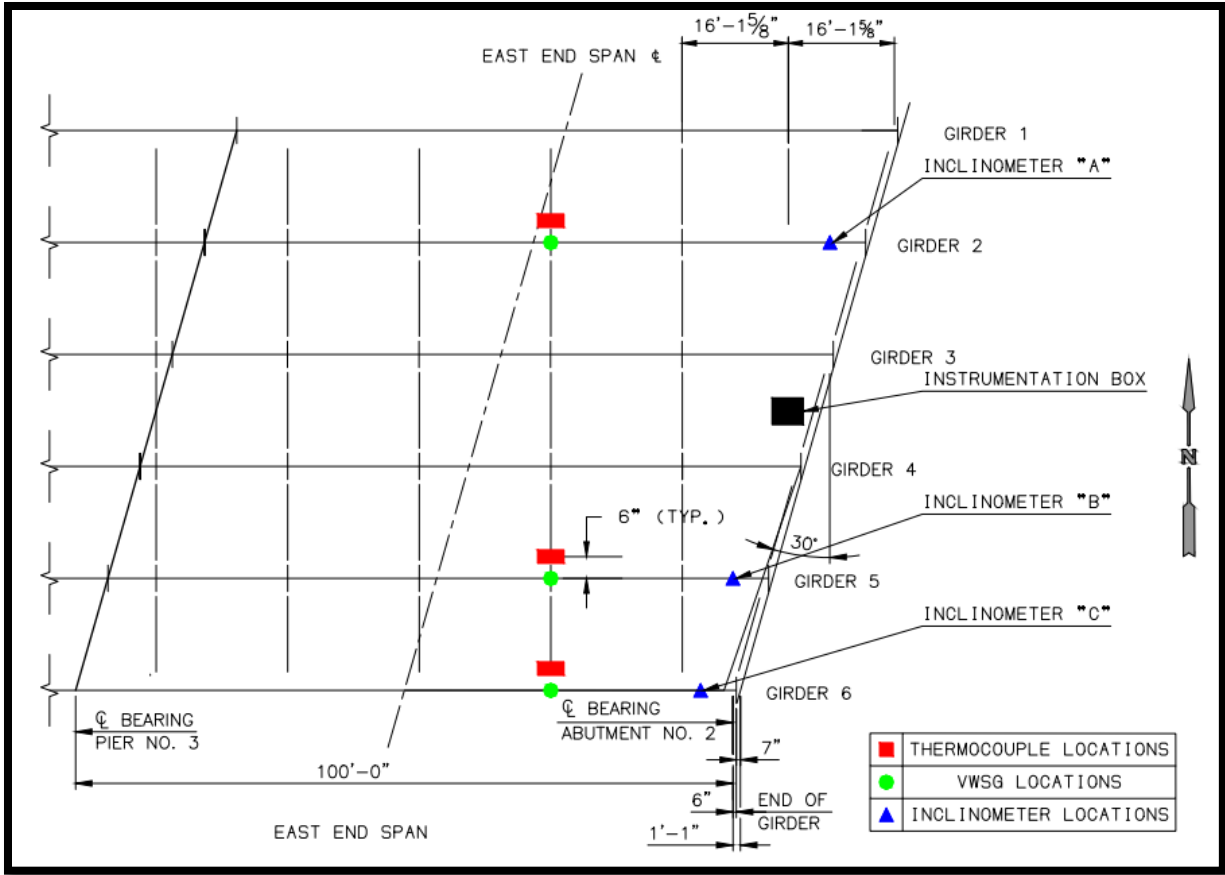
Figure 6.3: Sensor locations and girder numbers

6.2.6. Concrete Properties

The concrete deck pour was performed in two different phases. The first phase started with the concrete pour of the south side of the bridge on March 9th, 2020. The second phase started with the concrete deck pour of the south side on July 22nd, 2020.

6.2.6.1. Fresh Properties

The north span where our sensors were located was poured using five concrete mix trucks from PC Concrete in Ponca City, Oklahoma. The mixture used was the typical ODOT Class AA concrete mixture routinely used on concrete bridge decks across the state of Oklahoma.

Fresh properties testing was conducted on the second and third trucks to arrive on the jobsite. These two trucks provided the concrete that surrounded the sensors for the north deck. Slump, air content, fresh concrete temperature, and unit weight were determined for these trucks. The concrete was sampled directly from the mix trucks before it entered the concrete pump.

6.2.6.2. Hardened Properties

In addition to the fresh properties testing conducted on the two trucks mentioned above, 4"x8" cylinders and 4"x4"x11.75" shrinkage beams were also cast and initially cured onsite in accordance with ASTM C31. After 24 hours, the specimens were retrieved from the jobsite and

the cylinders were stored in the fogroom. The shrinkage prisms were stored in the drying room. The slump, air content, temperature, and unit weight data are shown in Table 6.1.

Table 6.1 - Fresh Concrete Properties by Truck

Concrete Property	Truck 2	Truck 3
Slump	5 1/4"	6"
Air content	5.5%	6.0%
Concrete Temperature (°F)	75.3	75.5
Ambient Temperature (°F)	61.8	61.8
Unit Weight (lb/ft^3)	141.7	144.1

6.2.6.1. Hardened Properties

Hardened properties testing was conducted at 2 days, 14 days, 28 days and 163 days. The hardened concrete properties for Truck 2 are shown in Table 6.2. Hardened concrete properties for Truck 1 are shown in Table 6.3.

Table 6.2: Hardened Concrete Properties from Truck 2 North Side -

Cast Date	3/9/2020			
Day	**2**	**14**	**28**	**163**
Date	**3/11/2020**	**3/23/2020**	**8/19/2020**	**8/19/2020**
C39 (ksi), Cylinder 1	2.90	5.21	5.90	6.58
C39 (ksi), Cylinder 2	3.24	5.39	6.33	6.43
Mean	3.07	5.30	6.12	6.51
S	0.24	0.13	0.30	0.11
Day	**2**	**14**	**28**	**163**
Date	**3/11/2020**	**3/23/2020**	**8/19/2020**	**8/19/2020**
C496 (ksi), Cylinder 1	0.37	0.66	0.29	0.37
C496 (ksi), Cylinder 2	0.37	0.53	0.49	0.50
Mean	0.37	0.60	0.39	0.44
S	0.00	0.09	0.14	0.09
Day	**2**	**14**	**28**	
Date	**3/11/2020**	**1/13/1900**	**8/19/2020**	
C469 (ksi), Cylinder 1	1670	3377	3367	
C496 (ksi), Cylinder 2	2608	3183	3328	
Mean	2139	3280	3348	

	Cast Date	3/9/2020			
Day	**2**	**14**	**28**	**163**	
Date	**3/11/2020**	**3/23/2020**	**8/19/2020**	**8/19/2020**	
S	663	137	28		

Table 6.3: Hardened Concrete Properties from Truck 1 South Side

	Cast Date	7/22/2020		
Day	**3**	**14**	**28,inside**	**28, outside**
Date	**7/25/2020**	**8/5/2020**	**8/19/2020**	**8/19/2020**
C39 (ksi), Cylinder 1	4.19	5.05	6.03	5.92
C39 (ksi), Cylinder 2	4.17	5.26	5.84	6.03
Mean	4.18	5.16	5.94	5.98
Stdev	0.01	0.15	0.13	0.08
Day	**3**	**14**	**28,inside**	**28, outside**
Date	**7/25/2020**	**8/5/2020**	**8/19/2020**	**8/19/2020**
C496 (ksi), Cylinder 1	0.41	0.50	0.51	0.41
C496 (ksi), Cylinder 2	0.41	0.44	0.3	0.40
Mean	0.41	0.47	0.41	0.41
Stdev	0.00	0.04	0.15	0.01

6.3.   Results:

6.3.1. Temperature Profiles

6.3.1.1.   Girders

Figure 6.4 and Figure 6.5 show the bridge recorded temperature over time. Figure 6.4 shows the recorded temperatures for Girder 5. Concrete was cast on July 22nd. We note that the ambient temperature during that cast was about 80˚F. This figure shows that the concrete temperature reaches 135 degrees peak temperatures at approximately 6:00 pm which is approximately 12 hours after the pour. We note that the deck was cast around 5:20 am in the morning. The concrete was in its induction state and dormant period until 8:00 am. Then, the concrete goes through an acceleration phase until it reaches its peak around 6:15 pm.
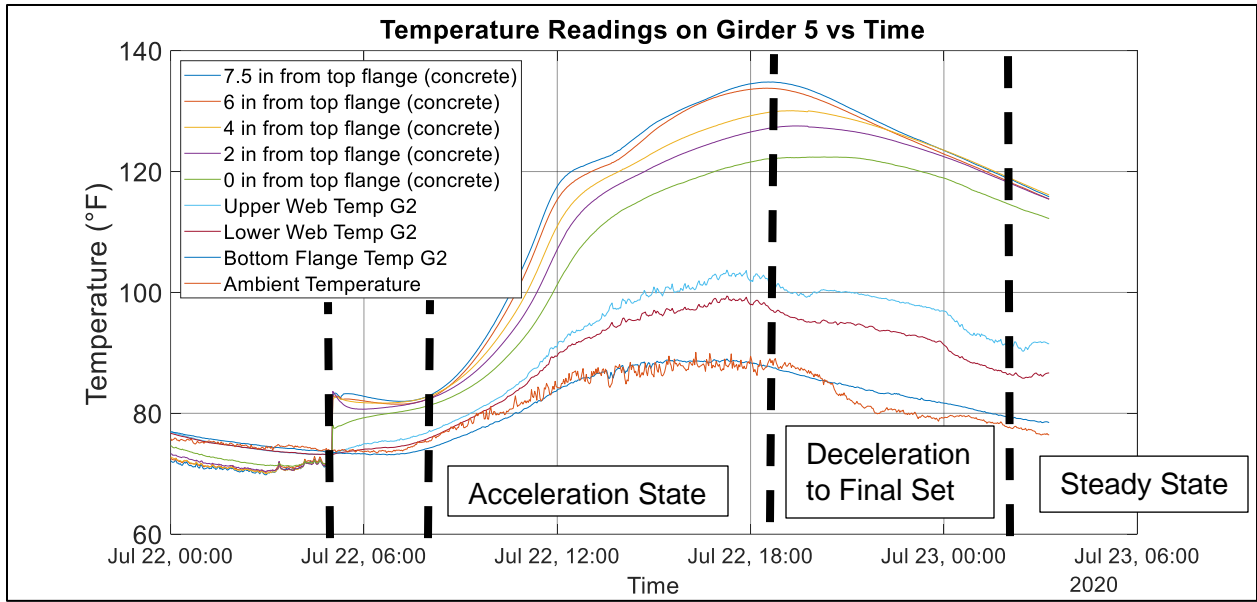
Figure 6.4: Temperature for 24h vs Time girder 5 (South Side)

For Figure 6.5 shows the recorded temperature for Girder 2 that was cast on March 9th. We note that the ambient temperature during that cast was about 60˚F. This figure shows that the concrete temperature reaches 135 degrees peak temperatures at approximately 6:00 pm which is approximately 12 hours after the pour. We note that the deck was cast around 10:00 am in the morning. The concrete was in its induction state and dormant period until 12:00 pm. Then, the concrete goes through an acceleration phase until it reaches its peak around 9:00 pm.
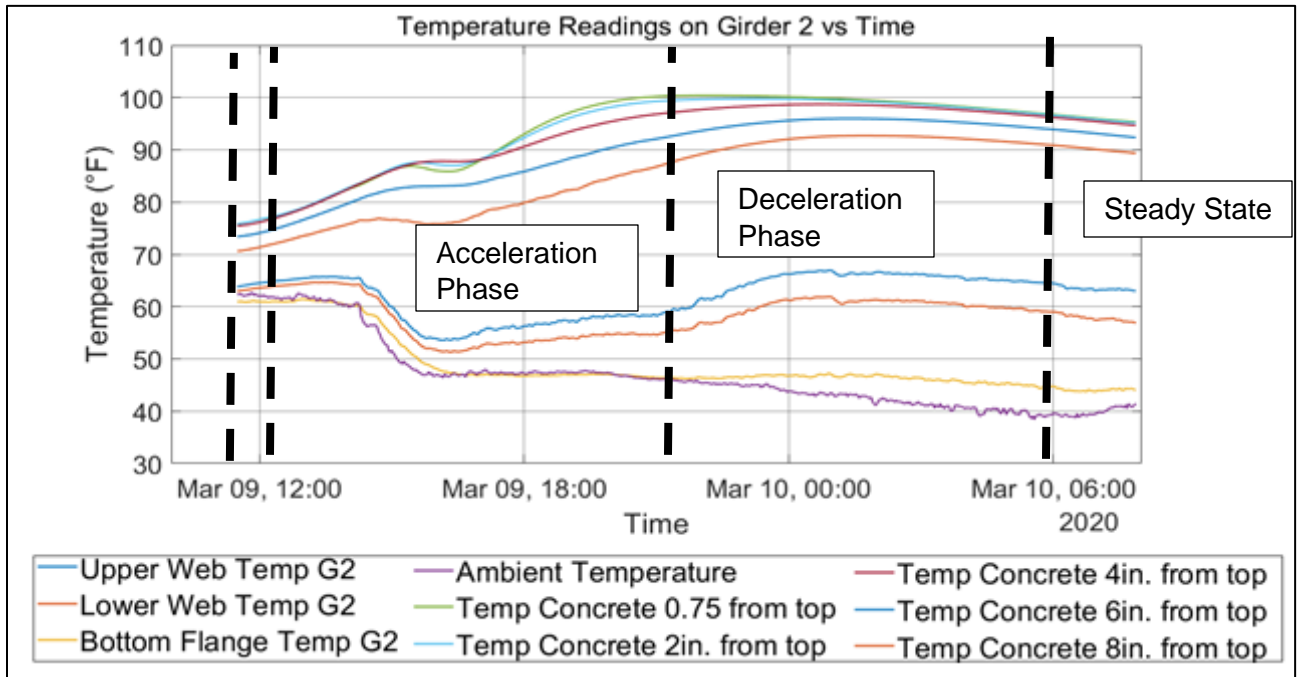

Figure 6.5: Temperature for 24h vs Time girder 2 (North Side)

59

We note that there is a difference between the deck temperatures of both pours (the north side and the south side of the bridge). The concrete temperature during hydration is affected by the ambient temperature. For the north side pour the peak temperature was about 100 degrees F while the ambient temperature was 60 degrees F. However, for the south side pour the peak temperature was recorded to be 135 degrees F while its ambient temperature was about 85 degrees.

6.3.1. Strain Profiles
6.3.1.1. Girders

Figure 6.6 shows the strain measurements for Girder 5 for the first 48 hours. We note that some data was lost because the solar panels were stolen, and the batteries required manual recharging.
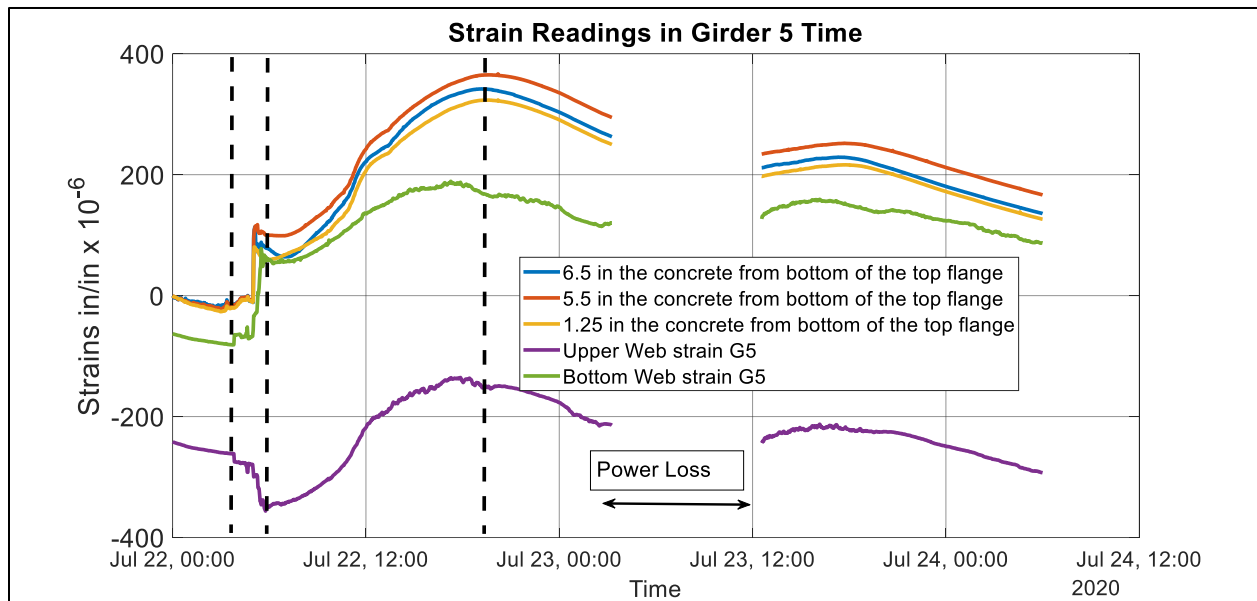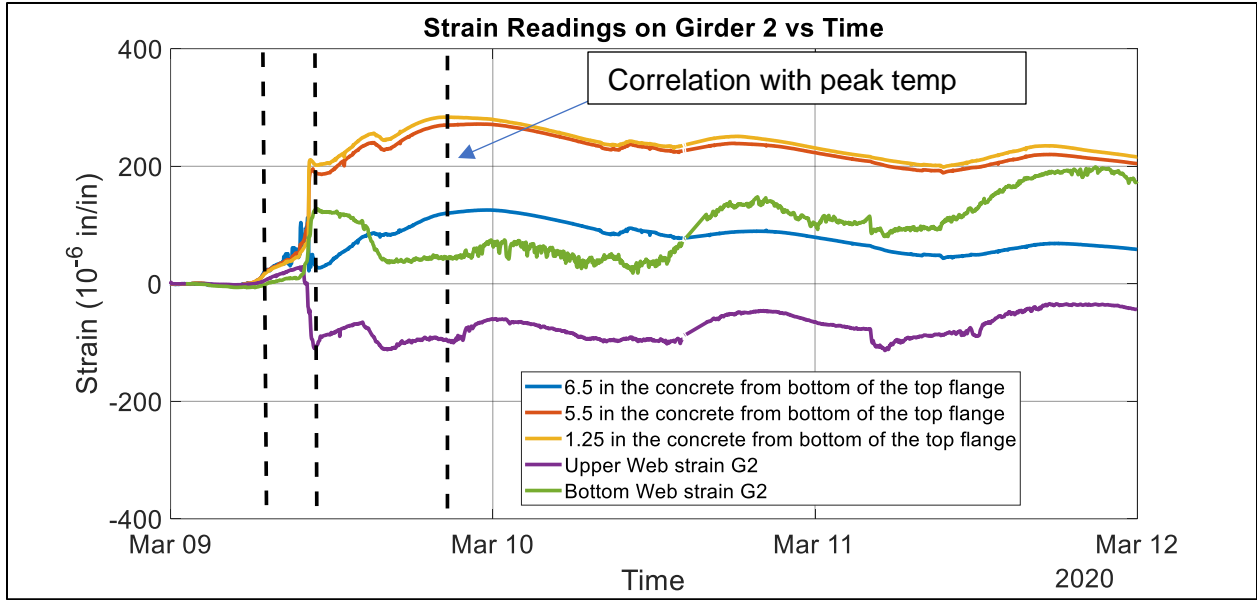

Figure 6.6: Strain vs Time in Girder 5

Figure 6.7 shows the strain measurements for Girder 2 for the first 48 hours. We note that data is continuous through the time period.

Figure 6.7: Strain vs Time in Girder 2

Figure 6.8 displays strain readings on Girder 2 from the cast date to present. It is observed that the girder is in compression, as opposed to tension. This is due to temperature differentials putting the sensors into compression. One can also see the seasonal cooling – temperature drops into the fall and winter months.
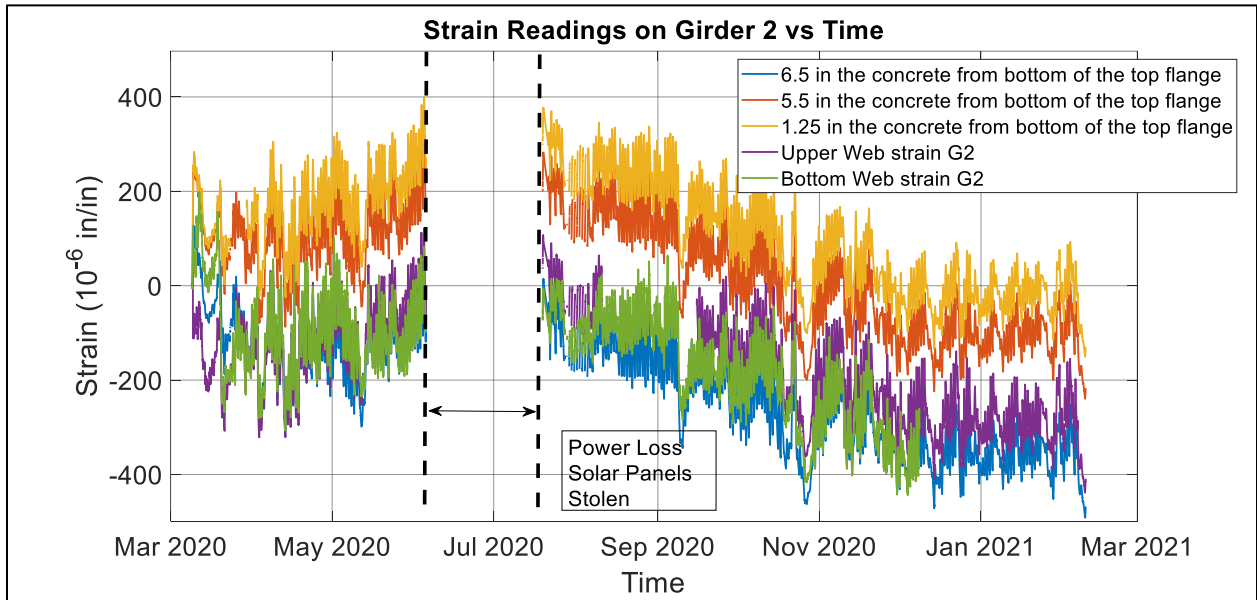
Figure 6.8: Strain Readings in Girder 2 since Deck Cast March 9th, 2020.

Figure 6.9 displays strain readings on Girder 6 from the data concrete was cast until February 2021. It is observed that the girder is in compression, as opposed to tension. This is due to temperature differentials putting the sensors into compression. One can also see the seasonal cooling – temperature drops into the fall and winter months.
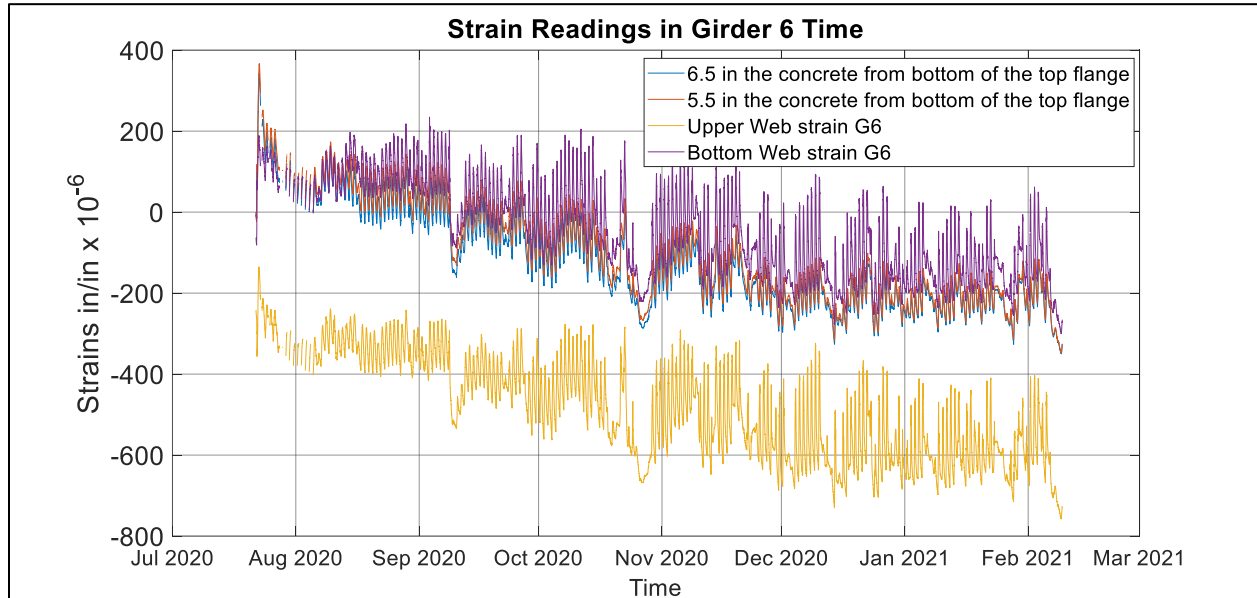

Figure 6.9: Strain Readings in Girder 6 since Deck Cast July 22nd, 2020.

6.3.2. Temperature Readings during extreme weather conditions:

In February 2021, Oklahoma saw extreme temperature fluctuations. A key part of our Task Order is to monitor Temperatures and Concrete strains. The data from Figure 6.10 show concrete, steel, and ambient temperatures during the month of February.

As shown, the SH 11 Bridge experienced more than 80 F temperature fluctuation during the month. The high temperature of 78 F occurred on February 23 just seven days after the concrete's low temperature of -4 F on the morning of February 16. Ambient temperatures reached a low of about -9 F. Additional data are shown in Figure 6.11.

Figure 6.11 shows the concrete strain data from SH 11 Bridge girder 5 in February 2021. The ambient temperature is also shown in the figure for the purposes of direct comparison. One can see in the data that the temperature fluctuation that occurs daily, and also through the weather cycles indicate that concrete and steel are shortening (increasing negative strains) when the temperatures become colder. From a monitoring point of view, there are several things that are

important to point out:

- Daily temperature fluctuations are typically varying +/- 20 to 30 F in a single day. The daily temperature fluctuations directly result in +/- 130 microstrains within the concrete material.
- Note that the measured strain is consistent with the change in temperature multiplied by the approximate coefficient of thermal expansion, $\alpha \approx 6.5 \times 10^{-6}$ in/in/F. So, a 20 F

change in temperature would produce +/- 130 microstrains. This is consistent with the data.

- Note that the daily change in strains is a reflection throughout the depth of the cross section. So, if the bridge experiences daily fluctuations of 150 microstrains, then that represents a change in length for the bridge girder of approximately 0.18 in. per span. There may be some independent data on girder movement, but this daily change in length is not widely reported. Obviously, support conditions (neoprene bearing pads, and other supporting hardware) must accommodate the daily change in length.
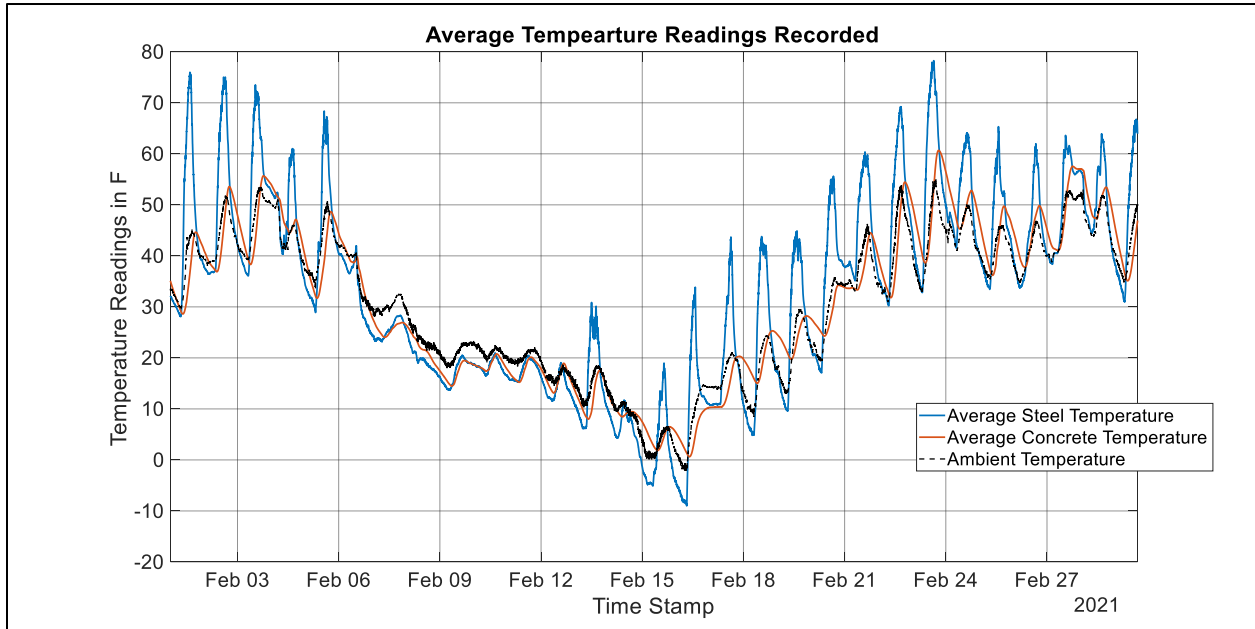
Figure 6.10: Steel and Concrete and Ambient Temperature Record for February 2021, SH 11 Bridge, Blackwell Co., OK
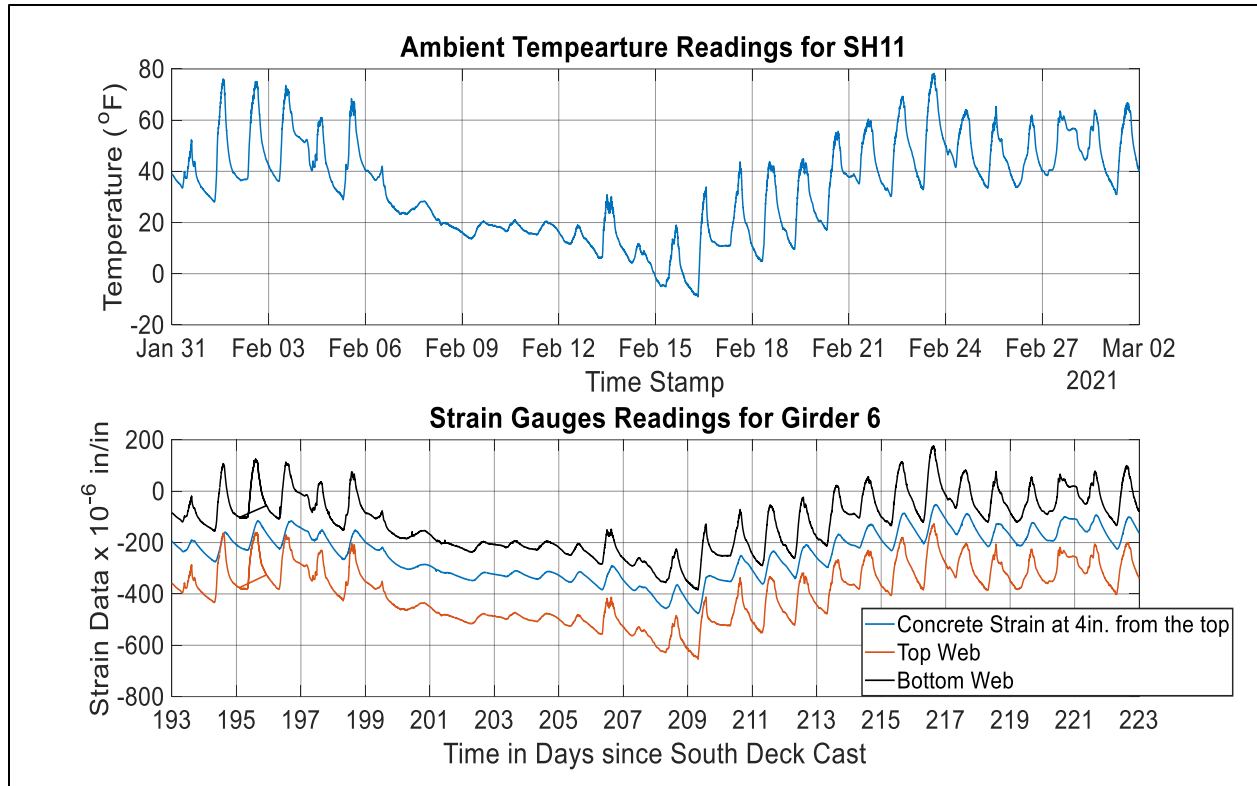
Figure 6.11: Steel and Concrete Strains Due to Extreme Weather Changes. Note that @ time = 193 days is compatible with January 31st, 2021. Note that the time = 0 is equivalent to July 22nd, 2020 (Concrete deck cast of the south side of the bridge)

6.3.3. Temperature Gradients:

Figure 6.12 and Table 6.4 show the average maximum temperatures measured at regular time intervals throughout the depth of the superstructure of girder 2. Temperatures were recorded at 2 min intervals. Figure 6.12 illustrates the

Figure 6.12 also illustrates the 12°F temperature gradient that occurs with the 8 in. concrete deck after 9hrs. of heating. Note also that temperature within the entire cross section increases, but that the steel temperatures are considerably smaller than concrete temperatures. The measured temperature gradient clearly exhibits non-linear temperature changes throughout the depth of the superstructure.
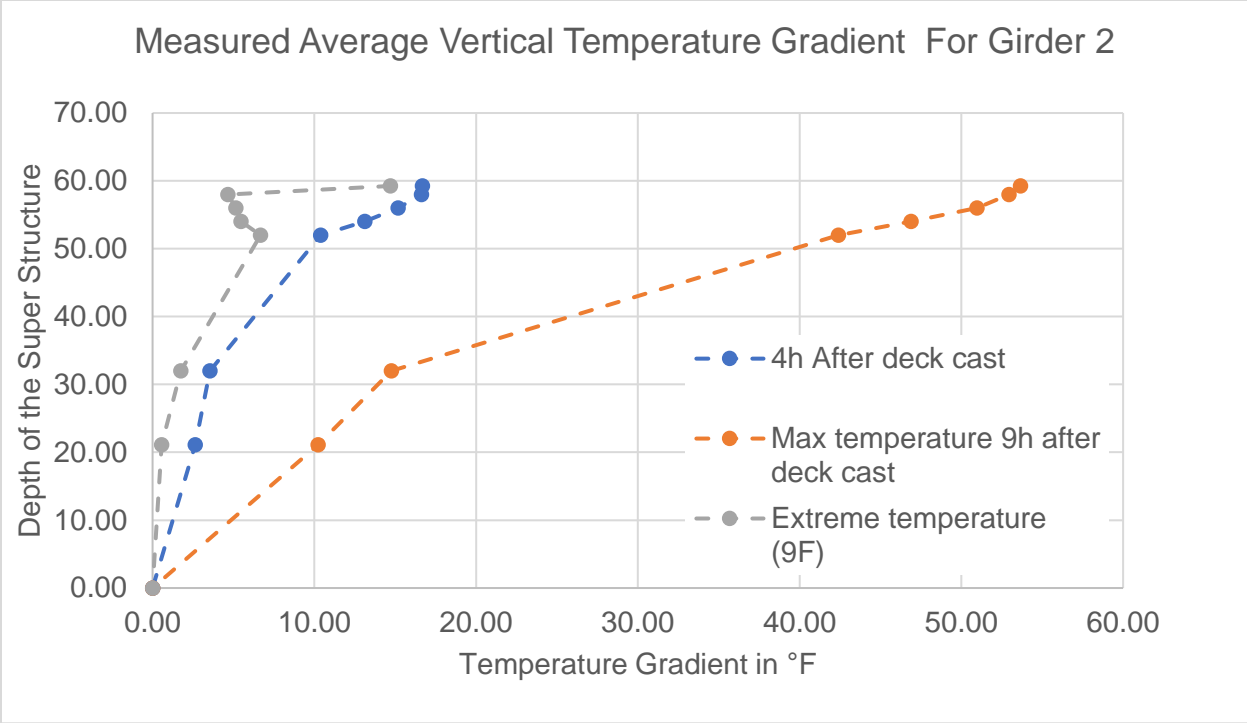
Figure 6.12: Measured Average Positive Vertical Temperature gradient for Girder 2

Table 6.4: Measured Average Positive Vertical Temperature gradient for Girder 2 – Temperature Readings and Temperature Gradients

Location From Bottom Flange	4h		Max Temp		Lowest Temperature	
y (in)	Temp	Gradient	Temp	Gradient	Temp	Gradient
59.25	77.66	16.68	100.40	53.66	5.10	14.70
58.00	77.60	16.62	99.68	52.94	-4.94	4.66
56.00	76.15	15.17	97.70	50.96	-4.45	5.15
54.00	74.10	13.12	93.63	46.89	-4.13	5.47
52.00	71.37	10.39	89.15	42.41	-2.92	6.68
32.00	64.53	3.55	61.50	14.76	-7.85	1.75
21.13	63.61	2.63	56.98	10.24	-9.04	0.56
0.00	60.98	0.00	46.74	0.00	-9.60	0.00

7. Conclusions:

7.1. Conclusions From Forensic Investigation and Overhang Bracket Testing:

The following conclusions are drawn from this research chapter:

Elevation surveys using conventional surveying equipment (i.e., engineering level and leveling rod) are effective in determining bridge deck driving elevations, for determining elevations at the bottom of the bridge decks and for determining bridge deck thickness without destruction testing

Measured roadway elevations showed measurable and significant "dips" in elevation profiles for two of the three bridges examined. Elevation profiles indicate a pattern where driving surfaces are significantly lower at the mid-spans of recently rehabilitated steel girder bridges. Bridge deck elevations "dipped" about 1.0 in. and as much as 1.75 in. in some bridge profiles. These data are reported, and the conclusions confirmed in Table 4.1 and Fig. 4.3 for the S.H. 14, Woods Co. Bridge, and in Table 4.4 and Fig. 4.7 for the SH 86, Payne Co. Bridge.

Measured roadway elevations confirm that the top surfaces of the bridge decks were screeded and finished in accordance with the 1 percent super-elevation required in construction documents.

- Under-slab elevations reflect the same 1 percent super-elevations measured on the bottom sides of the bridge decks from CL to the exterior girder; however, from the exterior girder outward and including cantilevered formwork, the under-slab elevations indicate a significantly steeper slope on the bottom surfaces of the slab. In the case of the SH 86 bridge, slopes exceeding 4.0 percent were measured on the bottom side of the deck slab. This is shown in Fig. 4.6 for the SH 86, Stillwater Creek Bridge.
- Bridge Deck thicknesses reported in Table 4.3 (SH 14 Woods Co. Bridge) and Table 4.6 (SH 86 Payne Co. Bridge) are significantly thinner than the 8 in. thickness required by contract documents. On the SH 14 Bridge, deck thickness as little as 7.25 in. was measured by instrument and verified by direct measurements. On the SH 86 Bridge, a slab thickness of 0.57 ft. or 6-7/8 in. was measured at midspan of the northern-most span.
- In contrast, bridge deck elevations measured on the US 281 Woods Co. Bridge show no elevation dips in the driving surfaces, and thicknesses measured by instrument showed actual concrete deck thicknesses varied from 8-1/8 in. to 8-7/8 in.
- In the case of SH 14, Eagle Chief Creek Bridge and of SH 86, Stillwater Creek Bridge, the formwork that was cantilevered outside of the exterior girder, and braced against the exterior girder, was not properly supported nor braced during construction activities. This conclusion is supported by the following forensic evidence:
  - Significant "dips" in driving surface elevations measured on both bridge decks,
  - Thin deck sections measured in both bridges.
  - Significantly severe slopes measured on the bottom sides of bridge decks, in areas that were supported by cantilevered formwork, which was in turn supported bracing.

- o For SH86 Bridge, the top side super-elevation from CL to Guardrail was 0.16 ft (2.0 in. on the northbound side, and 0.11 ft (1.375 in. on the southbound side. This compares to the under-slab elevation change from CL to Slab Edge of 0.32 ft. (3.8 in., northbound) and 0.29 ft. (3.5 in., southbound). These elevation differences directly correspond to "dips" in roadway elevations in excess of 1 in. and in thin bridge decks.
- Laboratory investigations confirm that commercially available bracing used for bridge rehabilitations is insufficient to provide necessary elevation controls for cantilevered portions of the bridge decks.

7.2. Conclusions From Full Size Prototype Bridge Instrumentation:

I. Heating of the concrete deck occurred in the first 14 hours from deck placement. Maximum temperature achieved was 114 ºF at 14 hrs. Concrete temperatures returned to ambient temperatures approximately 96 hrs. after concrete placement began.

II. Data show heating of the concrete deck placement at early ages causes upward deflection of the steel girder-composite concrete bridges. Likewise, the data show that the bridge deflected downward as the concrete cooled. Also, data show that differential shrinkage through the depth of the deck cause permanent variations in normal strain through the depth of the concrete deck.

III. Midspan deflection caused by the weight of fresh concrete was measured at 0.38 in. on one girder and 0.40 in. on the other. This deflection closely matched the beam theory computation of 0.42 in.

IV. Upward deflection caused by the elevated curing temperature of the concrete deck was approximately 0.071 in. Maximum upward deflection occurred at approximately 12.0 hrs. after concrete placement started whereas concrete temperatures occurred at approximately 14.0 hrs.

V. Concrete reached its ambient temperature at approximately 96 hrs. after deck placement. The overall midspan deflection at 96 hrs. was 0.48 in. downward on one girder and 0.50 in. on the other. In approximate terms, the total deflection is caused by two factors: 0.38 in. of downward deflection can be attributed to self-weight with slab cooling and shrinkage accounting for the remaining an additional 0.1 in.

VI. Concrete shrinkage and measured deflections of the full-size prototype beam indicate that shrinkage of concrete contributes to permanent downward deflections in composite bridge girders. The amount of measured permanent deflection attributed to shrinkage is approximately 0.1 in. at 28 days. However, it is noted that shrinkage beyond 28 days is not reported in this article.

VII. Early age temperatures in concrete correlates with the strains and deflections in the prototype beam. The increase in concrete temperature due to heat of hydration of cement has a significant effect on concrete strains. Concrete thermal strains increase with increasing temperatures causing the beam to deflect upward slightly.

VIII. The research indicated that wet curing time of bridge deck significantly reduced the rate of shrinkage of concrete, thereby reducing excessive deflections and helping to mitigate the formation of cracks in the bridge deck. It was observed that shrinkage strains and related downward bridge deformations accelerated after wet curing was removed at 14 days.

IX. High temperatures developed in concrete due to heat of hydration induces compressive stresses in the deck slab.

X. Poorly braced or inadequate overhang bracing systems cause excessive deformations in bridge overhangs and can affect the overall ride quality of bridge girders.

XI. The addition of flyash to concrete mix is found to reduce concrete temperatures during hydration thereby causing the reduction in shrinkage strains in concrete.

XII. Despite the compression stresses developed in concrete due to peak hydration temperatures, the stresses are quickly transformed to tensile stresses during the cooling cycle.

XIII. In field conditions where the temperatures are higher, or where shrinkage of concrete is higher, the tensile stresses within the deck could be enough to cause bridge deck cracking.

XIV. Simple computational approach can be used to calculate thermal, and shrinkage induced stresses in composite bridge girders.

XV. Early age cracking in bridge decks due to high shrinkage stresses in concrete can be reduced by using concrete mixes with low shrinkage and high tensile strength.

7.3. Conclusions From Material Testing:

From the results above, creep and shrinkage effects can clearly have a considerable impact on the strains experienced by the concrete, even at early ages. While creep is often relegated to the realm of long-term concerns, these results show that it still can result in strain values large enough that they cannot simply be ignored. The NOFA tensile creep coefficient was several times larger than its compressive counterpart, while the LWCM mixture's coefficients were relatively close between both load types, and the OPT mixture's compressive creep coefficient dwarfed its tensile coefficient. However, the compressive creep coefficient was quite similar between all four of the mixes. In the case of net strains, even the NOFA mixture did not exceed 150 microstrain in tension (compared to over 600 microstrain in its compressive creep test). This indicates that the compressive creep strain is a source of more concern than the tensile creep strain, at least in absolute terms. This is likely due to the fact that the initial strains applied to the dogbone specimens were much smaller than the one applied to the compression cylinders.

Also worthy of consideration is the fact that the mixtures with the highest compressive creep coefficients also had the lowest tensile creep coefficients. This casts further doubt upon the theory that creep is almost entirely a function of mixture properties (such as compressive strength or mortar composition) and is largely independent of the method of loading. Instead, it appears that the effects of tensile loading on the microstructure of young concrete can have dramatically different effects upon the creep it experiences.

For the comparison between tensile and compressive modulus of elasticity, it is clear that the 1-day tensile modulus is significantly higher than the compressive modulus for each mixture, regardless of the method of determining the compressive modulus. The extent of the difference between the two depends upon the mixture design and composition. This effect was observed at 7 loading as well, but for the 28-day loading the values were essentially equal. This observation could prove useful in predicting early-age cracking in concrete, as cracking is a result of excessive tensile stress. A better understanding the tensile modulus can provide an avenue to more efficient structures and designs.

7.4. Conclusions from Field Bridge Monitoring:

Results and findings from Structural Health Monitoring of SH11 bridge:

I. The beams acted composite after 24 hours of the casting of the girders.
II. Overall, we were able to remotely access the data logger throughout the year.
III. We were able to get real time data (Concrete temperature and concrete strain data).
IV. We have noticed temperatures have a large effect on strains measured in the steel girders.
V. The monitoring of te strains values of each girder can be used to evaluate the distribution factors on the bridge.
VI. Monitoring the neural axis location, can provide information about the condition of the deck. For example, if the deck starts to deteriorate the composite action will change.
VII. This research has shown that the continued monitoring of this bridge will provide data that can be used to determine if there are major changes in the structural integrity.

8. Recommendations:

8.1. Recommendation From Forensic Investigation and Overhang Bracket Testing:

1. The contract documents should specify that the contractor is responsible for means and methods of supporting bridge decks during construction.
2. The contract documents should specify that the contractor is responsible for maintaining limits on formwork and bracing deflections during construction.
3. The contract documents should specify that the contractor is responsible for roadway elevation profiles and deck slab thicknesses.
4. The Transportation Official's drawings and specifications should remove all references to prescriptive information regarding means and methods for deflection controls.
5. We recommend that the Transportation Official establish a tolerance limit on roadway elevation profiles, and that these elevation profile requirements should be enforced through bonus/penalty contract language.
6. We recommend that the Transportation Official establish tolerance limits and performance criteria for bridge deck thicknesses, and that these bridge deck thickness requirements should be enforced or promoted through bonus/penalty contract language.

9. Appendices – Published Journal Papers

9.1. Jayaseelan, H., Russell, B.W., Abdelmeguid, I.S., and Belcher, K. (2022). **Investigation of Poor Ride Quality in Steel Bridge Girders Made Composite with Concrete Decks** (Submitted to the *Journal of Performance of Constructed Facilities*)

9.2. Jayaseelan, H., Russell, B.W., and Webb, A.C. (2019). **Early Age Deflections in Newly Rehabilitated Steel Girder Bridges Made Composite With Concrete Slabs,** *Structural Engineering International,* 29:4, 575-585, https://doi.org/10.1080/10168664.2019.1605326.

9.3. Jayaseelan, H., Russell, B.W., and Webb, A.C., **Impact of Thermal Stresses on the Performance of Steel Girder Bridges Made Composite with Concrete Slabs,** 4:1, 8-29. https://iaeme.com/Home/issue/LJSE?Volume=4&Issue=1.